5-2018

Mixing by Cutting and Shuffling a Line Segment: The Effect of Incorporating Diffusion

Mengying Wang
Purdue University

MIXING BY CUTTING AND SHUFFLING A LINE SEGMENT: THE EFFECT OF INCORPORATING DIFFUSION

A Thesis

Submitted to the Faculty

of

Purdue University

by

Mengying Wang

In Partial Fulfillment of the

Requirements for the Degree

of

Master of Science in Mechanical Engineering

April 2018

Purdue University

West Lafayette, Indiana

THE PURDUE UNIVERSITY GRADUATE SCHOOL
STATEMENT OF THESIS APPROVAL

Dr. Ivan C. Christov, Chair

School of Mechanical Engineering

Dr. Guang Lin

Department of Mathematics

Dr. Aaron B. Morris

School of Mechanical Engineering

Approved by:

Dr. Jay P. Gore

Head of the School Graduate Program

ACKNOWLEDGMENTS

The author would like to thank Professor Ivan C. Christov for all his guidance throughout this project.

The majority of the work in this thesis has been submitted for publication.

TABLE OF CONTENTS

LIST OF TABLES

LIST OF FIGURES

Figure Page

ABSTRACT

Wang, Mengying. M.S.M.E., Purdue University, April 2018. Mixing by Cutting and Shuffling a Line Segment: The Effect of Incorporating Diffusion. Major Professor: Ivan C. Christov, School of Mechanical Engineering.

Dynamical systems are commonly used to model mixing in fluid and granular flows. We consider a one-dimensional discontinuous dynamical system model (termed "cutting and shuffling" of a line segment), and we present a comprehensive computational study of finite-time mixing. The properties of the system depend on several parameters in a sensitive way, and the effect of each parameter is examined. Space-time and waterfall plots are introduced to visualize the mixing process with different mixing protocols without diffusion, showing a variety of distinct and complex behaviors in this "simple" dynamical system. To improve the mixing efficiency and avoid pathological cases, we incorporate diffusion into this model dynamical system. We show that diffusion can be quite effective at homogenizing a "mixture." To make this effect clear, we compare cases without diffusion to those with "small" diffusivity and "large" diffusivity. Illustrative examples also show how to adapt mixing metrics from the literature, namely the number of cutting interfaces and a mixing norm, to quantify the degree of mixing in our cutting and shuffling system. To study the evolution of mixing through a large set of possible cutting and shuffling parameters, we introduce fit functions for the number of cutting interfaces and the mixing norm. These fits allow us to determined time constants of mixing for each different system considered, thereby quantifying the "speed" of mixing. Systems with various different permutations (shuffling protocols) are considered, then average properties can be computed, which hold true (on average) for all allowed permutations. The relationship between the fit parameters and the system parameters is also investigated through scatter plots in the fit parameter space. Next, universal mixing behaviors are identified by specifically introducing a critical half-mixing time, which must be found computationally. Using the latter, a rescaling of different

dynamical regimes (decay curves of the mixing norm) fall onto a universal profile valid across all parameters of the cutting and shuffling dynamical system. Then, a prediction for this critical half-mixing time is made on the basis of the evolution of the number of subsegments of continuous color (unmixed subsegments). This prediction, which is called a stopping time in the finite Markov chain literature, must also be found numerically. The latter compares well with the previously computed half-mixing time, which provides an approach to determine when a system has become uniform. Finally, we examine the dependence of the half-mixing times on the characteristic Péclet number of the system (an inverse dimensionless diffusivity), and we show that as the Péclet number becomes large, the system transitions more sharply from an unmixed initial state to a mixed final state. This phenomenon, which is know as a "cut-off" in the finite Markov chain literature thus appears to be well substantiated by our numerical investigation of cutting and shuffling a line segment in the presence of diffusion.

1. INTRODUCTION

Even simple discontinuous dynamical systems can exhibit highly nontrivial dynamics and mixing behaviors. One recently studied class of such systems are *piecewise isometries* (PWIs) [1–3]. Unlike the *stretching and folding* mechanism of chaotic fluid mixing [4], which is underpinned by horseshoe dynamics [4, 5] and is sometimes provably the "best" mixing possible [6], *cutting and shuffling* underlies granular mixing [7–10]. Cutting and shuffling, much like the "mixing" of a deck cards, involves breaking apart the material being mixed into discrete pieces and then putting it back together in a length-preserving (*i.e.*, isometric) way [11]. Mixing by cutting and shuffling via PWIs on non-Euclidean spaces (e.g., surface of a hemispherical shell) remains an active topic of research [12, 13]. Meanwhile, fluid mixing by stretching and folding dynamics in physical space is, by now, well-understood [4, 5, 14]. The interaction between stretching and folding and cutting and shuffling, on the other hand, remains a research frontier in the field of dynamical systems. As evidence for the latter point, we refer the reader to the detailed studies by Smith *et al.* [15–17] of shear maps coupled to discontinuous motions (such as "slip deformations"), showing a wealth of distinct types of dynamical behaviors including enhanced mixing and exotic bifurcations.

The simplest example of cutting and shuffling is the one-dimensional (1D) PWI known as an *interval exchange transformation* (IET) [21, §14.5]. Recently, a class of IETs relevant to granular mixing and their mixing properties were studied by Krotter *et al.* [19]. This IET construction and its requisite simulation methodology were introduced to model the intuitive process of cutting and shuffling a line segment. The reason for considering such apparently simple 1D dynamics is that they are arise in more complex mixing flows, often underlying the mixing behavior, as shown in Figure 1.1. Specifically, in Figure 1.1(a), a granular mixing simulation in a spherical tumbler is shown and, if we consider only the outer edge dynamics in the tumbler, the process can be idealized as a cutting and shuffling of a line segment after unwrapping the circle. After several time periods, the distribution of different materials

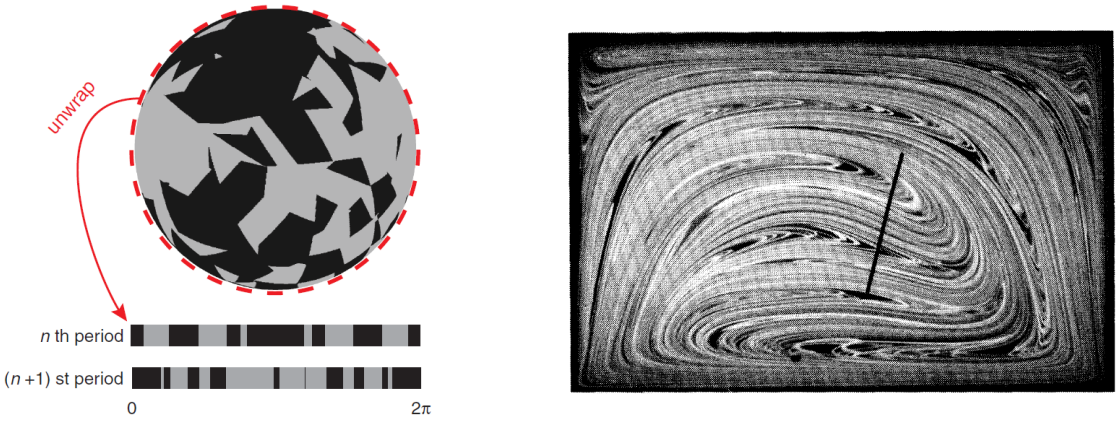

(a) (b)

Figure 1.1. (a) View from below of a piecewise isometry (PWI) simulation of mixing of two granular materials (black and gray) in a "blinking spherical tumbler flow" [10, 18]. Image in panel (a) reproduced, with permission, from [19] c 2012 World Scientific Publishing Co. (b) A lamellar structure can be sampled to generate an interval of different gray/black subsegments similar to (a). Thousands of striations of distributed thicknesses can be obtained by taking a cross-cut through the middle of a fluid undergoing mixing in a square cavity flow. Image in panel (b) reproduced, with permission, from [20] c 1989 American Physical Society.

can become randomized (mixed). Figure 1.1(b) shows another example of how 1D cutting and shuffling dynamics might emerge. A lamellar structure with striations of distributed thicknesses, which vary in time as the lamella interact, is produced by taking a cross-cut through the middle of a chaotic fluid mixing in a cavity flow. The evolution of distribution of materials along this one intersection can also be idealized as a cutting and shuffling process, perhaps with reaction and diffusion as well.

Yu *et al.* [22] extended the work in [19] to account for possible uncertainty in the location of cuts along the line segment, as might be the case when fractionating a granular material such as a powder. Consequently, the length of each portion of the cut and shuffled line segment is random, potentially leading to enhanced mixing. Most recently Smith *et al.* [23] introduced a new metric to quantify mixing by IETs, combining the length of the largest uncut subsegment and the evenness of color distribution across subsegments. They demonstrated that cutting in half the longest unmixed subsegment of distinct color at each iteration, which proves to be computationally inexpensive, can lead to optimal mixing in the sense of minimizing the proposed mixing metric. Such "optimal" mixing can also be achieved with a fixed shuffling protocol if the cut locations change at each iteration (beyond just the addition of uncertainty in cut locations as in [22]). Beyond the computational work of [19, 22], the mathematical theory of IETs is, in fact, quite daunting. The "weak mixing" properties of IETs were only recently established [24, 25] in work that required the development of abstract mathematical notions at such a high level that one of the authors of [25] (A. Avila) received the 2014 Fields Medal for his contributions to dynamical systems theory [26].

The IET construction introduced by Krotter *et al.* [19] has several parameters that can be varied to produce distinct mixing behaviors, including pathological poor-mixing cases that were examined in detail therein. Some connections between abstract mathematical notions of mixing and numerical experiments with IETs were also summarized in [19, 22], leading to several basic "design principles" for how to best cut and shuffle a line segment. Specifically, the number of cuts (subsegments, N, introduced in each cutting step) can be varied, the shuffling order (a permutation, Π, of the integers up to N) can be changed, and the lengths of each subsegment (parametrized by a fixed adjacent subsegment length ratio r) can be chosen so as to enhance mixing. In [19, 22], mixing was quantified through the percentage of the line segment's length that is unmixed (*i.e.*, the proportion of the line segment composed of the same continuous "color") or as measured by the number of cutting interfaces (*i.e.*, interfaces between different "colors" present). Yu *et al.* [22] additionally showed that even

slightly perturbing the cut locations stochastically can break periodicity in the system, again leading to mixing.

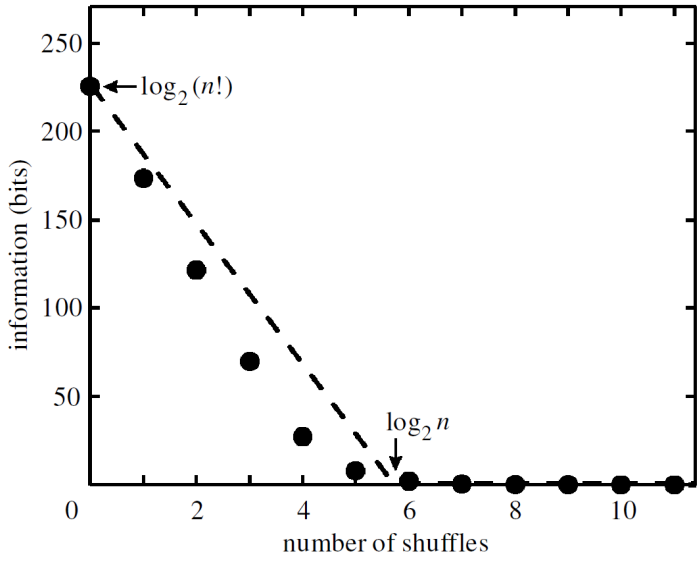

Figure 1.2. Information decay due to shuffling for a deck of fifty-two cards, showing how many shuffles are required to randomize it (*i.e.*, decrease the information content to zero). Image is reproduced, with permission, from [27] c 2000 The Royal Society.

Our study of cutting and shuffling is also motivated, in part, by the shuffling a deck of cards. Numerical results by Trefethen and Trefethen [27] illustrate a well-known phenomenon of "cut-offs" in card shuffling, as shown in Figure 1.2. Given the number of n cards to be shuffled, it has been shown that the number of shuffles required to reach total randomization scales as $\log_2 n$. In particular for $n = 52$ (a typical deck of cards), $\log_2 52 \approx 6$. Indeed, in the simulation from [27] shown in Figure 1.2, we see that the "amount of information" decays as the deck of cards is shuffled, reaching zero around 6 or 7 iterations. More specifically, it is known from work by Diaconis *et al.* [28–30], based on probability theory of finite Markov chains, that it takes about seven riffle shuffles to randomize a fifty-two card deck (see also

the *New York Times* article [31] on this fascinating result) [1]. Any further shuffling does not significantly improved the "mixedness" of the deck. Hence, seven shuffles represents a *stopping time* for the shuffling process, and the dynamical system exhibits a *cut-off* there, at which a sudden change in the mixedness of the cards from poorly to well mixed occurs, as shown in a schematic way in Figure 1.3 below (inspired by the illustration in [28, Figure 2]).

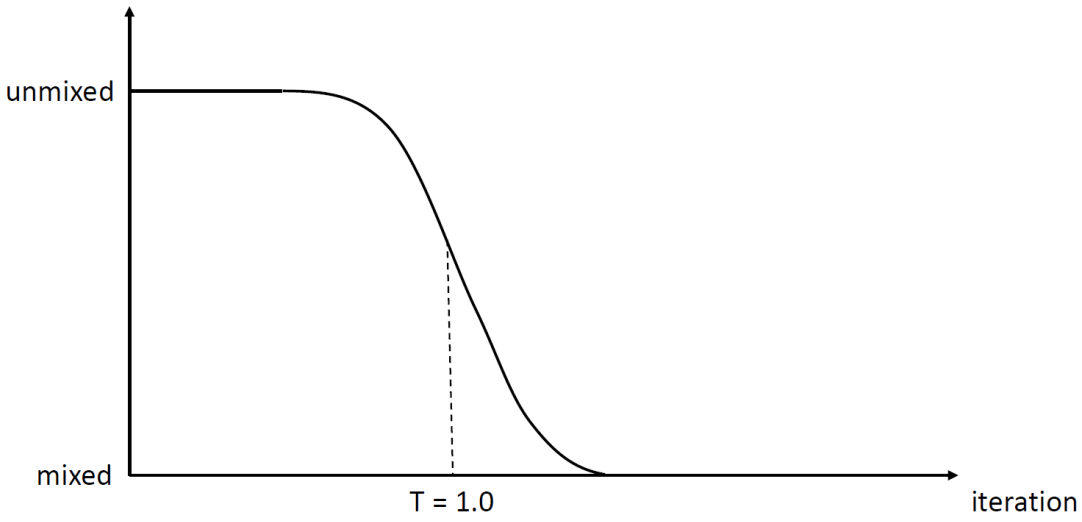

Figure 1.3. Cartoon diagram of a cut-off in a mixing process.

Recently, such cut-offs were demonstrated [33] through the numerical simulation of chaotic fluid mixing in a staggered-herringbone microfluidic channel [34]. By varying the Péclet number (an inverse dimensionless diffusivity), an appropriate global measure of "mixedness" can be rescaled and shown to fit the notion of a cut-off, just like in card shuffling. To this end, in this work, we incorporate diffusion into the one-dimensional cutting and shuffling process, and we address the existence of cut-offs in this model system. Understanding such admittedly "simple" systems that yet exhibit "complex" dynamical behavior can often be impactful for statistical [35] and material physics [36].

[1] A simple counting argument by Keller [32] provides a similar estimate of how the cut-off number of shuffles scales with the number of cards.

Though there have been a number of theoretical and computational studies of IETs, there is still much to be understood about the basic cutting and shuffling model discussed above. Just as Ashwin *et al.* [37] pointed out that "the mixing properties of interval exchange maps are very subtle and relatively poorly understood and depend on parameters in a sensitive way," our aim is to explore how different parameters influence the system's mixing behaviors and whether there is any "universality" in the phenomenon.

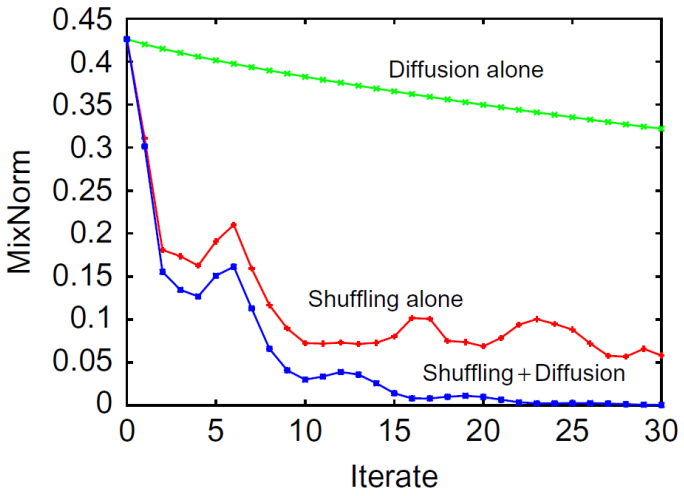

Figure 1.4. Combining a weakly mixing IET with diffusion creates a more efficient mixing process (as measured by how fast a "MixNorm" decays with iterations of the mixing protocol) than either cutting and shuffling by IET alone or mixing by diffusion alone. Image is reproduced, with permission, from [38] c 2012 Elsevier, Inc.

Going beyond the simple IETs of Ashwin *et al.* [37], Sturman [38] provides a comprehensive review of mathematical theories relevant to discontinuous mixing. Examples of IETs with diffusion were discussed in the context of simulating the mixing of a black-and-white line segment. By computing the decay of the so-called "MixNorm," as shown in Figure 1.4, mixing with diffusion alone or by cutting and shuffling alone was found to be much less effective than when the two mechanism were combined. Going further, Froyland *et al.* [39] proposed local perturbations to speed up mixing in various dynamical systems. Specifically, they sought to optimize how diffusion is added across the system, including one-dimensional

line segments undergoing cutting and shuffling. Dynamical system with different fixed diffusion protocols (termed "none," "uniform," "Gaussian," and "optimal") were compared [39], showing that optimizing the diffusion protocol leads to enhanced mixing at any Péclet number. Here, we consider only Gaussian diffusion.

Most recently, Kreczak *et al.* [40] studied a one-dimensional model of mixing of a line segment with a combination of stretching, permutations and diffusion. Their results show that the global mixing rate depends on both the choice of permutation and the diffusion coefficient. Contrary to expectation (and the results of Ashwin *et al.* [37]), increasing the diffusion coefficient leads to a *deceleration* of the mixing rate when *both* stretching and folding and cutting and shuffling are present. Given just four detailed studies [37–40] on this topic exist, the dynamics of cutting and shuffling a line segment in the presence of diffusion remain largely unexplored.

Our work aims to fill the latter knowledge gap in this field. After introducing the IET construction in Chapter 2, which is the basis of our cutting and shuffling model, we proceed to discuss in detail the effects of diffusion on cutting and shuffling in Chapter 3. Although many measures of mixing exists (see, *e.g.*, the detailed review [41]), including multiscale mixing norms [42], we use the definition of mixing norm introduced in [37] (Section 3.3), which determines how far the line segment's color distribution is from the uniform average color of the initial condition. Then, having quantified mixing, we verify that diffusion generically leads to decay of the mixing norm (Section 3.3). To explore the parameter space of this system and see how mixing proceeds under different protocols, we introduce a fit function for the decay of the mixing norm with the number of iterations (Section 3.3). Specifically, from the fit function, we extract a decay time constant for each protocol in the parameter space. Next, we define the "half-mixing time," which quantifies how many iterations it takes to reach the halfway point of the mixing norm decay. With the half-mixing time in had, in Section 3.4 we rescale the concentration/color mixing norm decay curves for different cutting and shuffling systems with diffusion to show that a universal mixing behavior exists. Then, in Section 3.5, we predict this critical number of iterations using the average length of unmixed subsegments of continuous color during cutting and shuffling and a Batchelor-

scale-type diffusion argument. We argue that, on the basis of these numerical results, there is strong numerical evidence for the existence of a cut-off phenomenon for IETs with diffusion, as we hypothesized. Finally, conclusions and avenues for future work are stated in Chapter 4.

2. SIMULATION METHODOLOGY

In this chapter, we describe the simulation methodology that we employ to study mixing of a line segment by cutting and shuffling, including incorporating the effect of diffusion. In Section 2.1, we defined a class of *interval exchange transformations* (IETs) that represent our cutting and shuffling protocols, and we also defined critical parameters to construct the dynamical system. In Section 2.2, the rules for choosing the parameters were clarified, including how to sort out good mixing cases and exclude pathological ones. In Section 2.3, two ways of quantifying the degree of mixing were introduced as cutting interfaces and the mixing norm, and we defined how to calculate them. In Section 2.4, we choose two types of plots to visualize the mixing process, which were space-time plot and waterfall plot. In the last Section 2.5, details of how to incorporating diffusion into the dynamical system were presented, which improved the mixing rate efficiently.

2.1 Parameters of the Model

The model of an IET construction of cutting and shuffling a line segment was shown in Figure 2.1. The behavior of this dynamical system sensitively depends on four parameters: the number of initial subsegments N, the length ratio between adjacent subsegments r, the shuffling permutation Π and the iterations T. The top row of Figure 2.1 shows how a line, of total length L, is divided into $N = 4$ subsegments at each iteration of this dynamical system, which represents the cutting process. Given this value of $N = 4$, the line is cut into N pieces and each piece is, additionally, given a distinct color. The color may, for example, represent different kinds of materials, or the same material but with different "concentration" of some tracer being mixed by cutting and shuffling. The ratio r is defined as the ratio of the lengths of adjacent subsegments, for example, r equals to the length of the second subsegment divided by the first subsegment, and also equals to the length of the third subsegment

divided by the second subsegment, while ξ is the length of the first subsegment. Therefore Figure 2.1 clearly shows that the initial length of each subsegment is ξ, $r\xi$, $r^2\xi$, $r^3\xi$, which is a geometric sequence. The permutation Π determines the rearrangement order, which represents the shuffling process. Figure 2.1 shows a specific example with $N = 4$, $r = 1.5$ and $\Pi = [3142]$. Here, we use the notation "[3142]" to denote the permutation that maps the integers [1234] to [3142] in that order. To be more specific, after cutting the line into four initial pieces, we put the third piece to the first place, the first piece to the second place, the fourth piece to the third place, and then the second piece to the last place. Therefore we finished one shuffling process with a specific permutation $\Pi = [3142]$. Here, we do not consider $N \geq 10$, so there is no fear of confusion in dropping the spaces between the integers in our notation. The cutting location remains the same at every iteration and subsegments are rearranged according to the same pattern. Then we could repeat the same cutting and shuffling process as many iterations as possible. Therefore we introduced the last parameter T as the iteration counter, which represents how long the cutting and shuffling process will last. In Figure 2.1, two iterations of the cutting and shuffling process are performed with the permutation $\Pi = [3142]$, so $T = 2$. And $T_{\max}$ refers to the total number of iterations of cutting and shuffling performed. The color map of Figure 2.1 is arbitrary, and the color values are normalized between 0 and 1 with equal interval, for example, if we have four colors ($N = 4$), the first and last color have a value of 0 and 1, the second color has a value of $1/3 \approx 0.333$, and the third color has a value of $2/3 \approx 0.667$.

As can be observed from the bottom row in Figure 2.1, when the number of iterations T increases, the number of subsegments of continuous color varies, often increasing. If we do not consider other factors, the number of subsegments of continuous color will increase then decrease, if the iterations are large enough, it always shows a periodic pattern as indicated in [19]. Figure 2.1 also highlights the two measures of mixing discussed in [19, 22]: the percent unmixed $U(T)$ (*i.e.*, the percent out of L corresponding to the longest continuous color subsegment, in Figure 2.1, the second white subsegment has the longest length of $0.23L$ at iteration 2, here $U = 23\%$ at $T = 2$) and the number of distinct cuts $C(T)$ (*i.e.*, interfaces

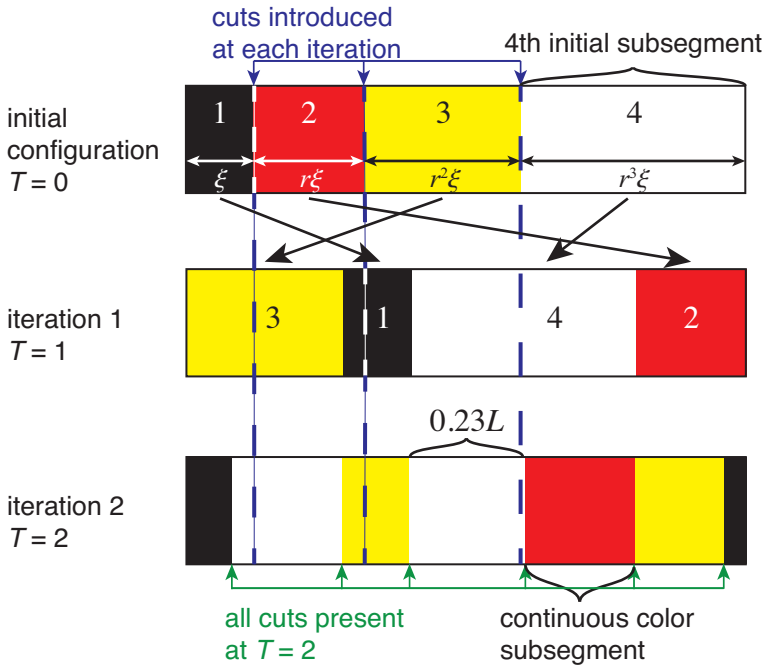

Figure 2.1. IET construction representing cutting and shuffling of a line segment. Here, a line segment is cut into $N = 4$ (in this case) line segments with adjacent length ratio r and initial subsegment length ξ. Two iterations of the cutting and shuffling process (without diffusion) are performed with the permutation $\Pi = [3142]$. Key terminology is labeled. The color map is arbitrary, and the color values are normalized between 0 and 1.

between distinct colors, in Figure 2.1 the number of interfaces between distinct color is 6 at iteration 2 as the green arrow indicated, here $C = 6$ at $T = 2$).

2.2 Choosing the Parameters: Design Rules

A major conclusion of Krotter *et al.* [19] was that mixing under this type of IET reaches a "point of diminishing returns" as N increases with four to five subsegments being sufficient to produce significant shuffling of the material. Thus, in the present work, we restrict our attention to the cases $N = 4$ and $N = 5$.

As discussed in [19] and further elucidated in [22], in choosing the shuffling permutation Π, we should exclude ones that lead to pathological behaviors. Based on the study of

Krotter *et al.* [19], irreducible permutations are the most practical for good mixing behaviors. Specifically, we exclude more pathological cases only consider permutations Π that are (i) irreducible, (ii) non-rotational, (iii) without the first or last element fixed, and *additionally* for the cases with $N > 3$, (iv) without a number of elements > 1 and $\leq N - 2$ being consecutive. For example, if $N = 4$, there are 24 possible permutations, however, only nine of them are "allowed" based on our rules: $\Pi = [2413]$, $[2431]$, $[3142]$, $[3241]$, $[3421]$, $[4132]$, $[4213]$, $[4312]$, $[4321]$.[1] In particular, $\Pi = [2143]$ is exclude by rule (i) for being reducible, *i.e.*, elements 1 and 2 are interchanged and 4 and 3 interchanged, splitting ("reducing") the permutation into two sub-permutations. Meanwhile, $\Pi = [2341]$ and $\Pi = [3412]$ are excluded by rule (ii) for being a rotation, *i.e.*, elements are shifted one to the right without significant re-arrangement. And $\Pi = [1423]$ and $\Pi = [3124]$ are exclude by rule (iii) with the first or last element fixed. Then, $\Pi = [4231]$ is excluded by rule (iv) because elements and 2 and 3 remain consecutive in the permutation.

Additionally, consonant with the available theory of IETs [43], Krotter *et al.* [19] showed that the initial cuts should break apart the interval in such a way that the adjacent segment length ratio r is "closer" to an irrational number. Moreover, it was concluded in [19] that the initial distribution of subsegment lengths should be "balanced," that is, r should be chosen close (but not equal) to unity. Thus, in the present work, without loss of generality, the ratio r is taken to be $r > 1$, then as shown in Figure 1.1, the total length L of the line segment is

$$L = \sum_{j=1}^{N} r^{j-1}\xi. \tag{2.1}$$

In order to realize the shuffling process within a MATLAB code, while ensuring length-preservation of the line segment without being subject to round-off errors, the initial lengths of *all* subsegments, *i.e.*, $\{\xi, r\xi, r^2\xi, \ldots, r^{N-1}\xi\}$, should *all* be integers. If the latter condition is met, then cuts *always* fall at unique indexes in the discrete array that represents the line segment computationally, which ensures that no length can be "lost" by rounding potentially

[1]For $N = 5$, the allowed permutation are [2 4 1 5 3], [2 4 3 5 1], [2 5 1 4 3], [2 5 3 1 4], [2 5 4 1 3], [2 5 4 3 1], [3 1 5 2 4], [3 1 5 4 2], [3 2 5 1 4], [3 2 5 4 1], [3 5 1 4 2], [3 5 2 1 4], [3 5 2 4 1], [3 5 4 2 1], [4 1 3 5 2], [4 1 5 3 2], [4 2 1 5 3], [4 2 5 1 3], [4 2 5 3 1], [4 3 1 5 2], [4 3 2 5 1], [4 3 5 2 1], [5 1 3 2 4], [5 1 4 3 2], [5 2 1 4 3], [5 2 4 1 3], [5 2 4 3 1], [5 3 1 4 2], [5 3 2 1 4], [5 3 2 4 1], [5 4 1 3 2], [5 4 2 1 3], [5 4 3 2 1].

fractional indexes up or down. To restate this important point: by guaranteeing that cuts fall at unique array elements, then we automatically ensure that the line segment's length cannot change, *i.e.*, we enforce conservation of mass.

To ensure that the subsegment lengths $\{\xi, r\xi, r^2\xi, \ldots, r^{N-1}\xi\}$ are all integers, we convert r to a fraction as r_n/r_d, where r_n is the nominator (an integer) and r_d is the denominator (also an integer). This conversion is always possible as long as r is a rational number. Since, in MATLAB, we use finite-precision floating point arithmetic, then any r we could pick must be representable as a fraction, though it might be quite a "complicated" fraction. Now, once we have written $r = r_n/r_d$, it is clear that multiplying the list $\{1, r, r^2, \ldots, r^{N-1}\}$ by r_d^{N-1} yields a set of integers with greatest common divisor 1. Thus, we conclude that

$$\xi = r_d^{N-1} \tag{2.2}$$

will guarantee that every subsegment's length is an integer. Finally, substituting the expression for ξ from Equation (2.2) into the total length of the line given in Equation (2.1), we find that

$$L = \sum_{j=1}^{N} r^{j-1} r_d^{N-1} = \left(\frac{1 - r^N}{1 - r}\right) r_d^{N-1}. \tag{2.3}$$

In plots, we will generally normalize the horizontal axis by L so that the line segment $[0, L]$ becomes the interval $[0, 1]$, and subsegments' positions along this unit interval are displayed.

In particular, we conclude that L only depends on N and r for a given cutting and shuffling protocol for our integer-arithmetic IET construction. Figure 2.2 shows the relationship between different L, N and r as predicted by Equation (2.3). For larger number of subsegments N, the total length L increases by orders of magnitude (note the logarithmic vertical scale in the figure), while maintaining that same periodic pattern. The smallest integer L occurs for the ratio $r = 1.5$ for all three values of N. Also, notice the sensitive dependence of L on r, which is likely fractal (becomes more complex as more values of r are added). Specifically, if we have a system with $N = 5$ subsegments and ratio $r = 1.2$, the total line segment length L that we consider is $\left(\frac{1-1.2^5}{1-1.2}\right) \times 5^4 = 4651$. In plots, we will generally normalize the horizontal axis by L so that the line segment $[0, L]$ becomes the interval $[0, 1]$, and subsegments' positions along this unit interval are displayed.

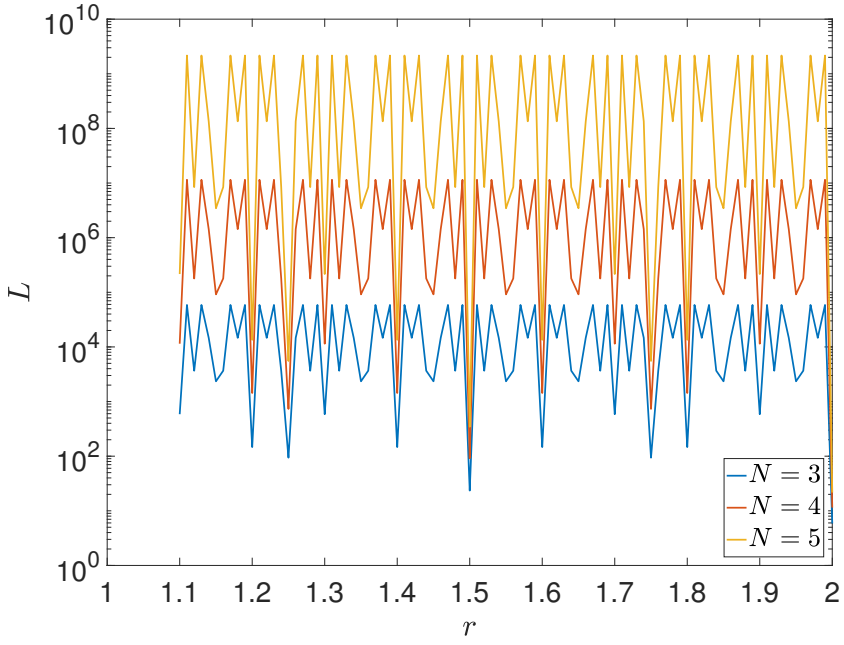

Figure 2.2. Relationship between the total segment length L (when using integer arithmetic to ensure cuts coincide with array elements) and the subsegment length ratio r for three choice of initial subsegment counts ($N = 3$, 4 and 5).

2.3 Quantifying Mixing: Cutting Interfaces and the Mixing Norm

After T iterations of the cutting and shuffling map, the initially coherent sets of colors assigned to the pieces of the line segment can form a complex and intricate pattern [19, 22]. There are many measures of mixing that can be used to quantify the *degree of mixing* produced by cutting and shuffling. On the one hand, there are discrete measures such as counting the number of distinct cuts between different colors, as discussed earlier. On other hand, there are a variety of so-called "mixing norms" that can be used to quantify the degree of mixing in a more "global" way, as discussed in the review by Thiffeault [42]. In this work, we will utilize the number of cuts $C(T)$ and the L^p function-space norm, denoted $||c||_p(T)$, to quantify mixing.

As discussed in Section 2.1, the number of cutting interfaces $C(T)$ refers to the number of distinct interfaces between two different continuous color subsegments after T iterations.

This is a clear and intuitive metric of how much rearrangement our cutting and shuffling protocol has achieved. Taking Figure 2.1 as an example, after the first iteration, there are 3 interfaces since 4 subsegments are generated, therefore $C(1) = 3$. After the second iteration, there are 6 interfaces between distinct components, therefore $C(2) = 6$. Given a color distribution $\{c_i\}_{i=1}^{L}$ across the line segment (represented by the lattice $i = 1, 2, \ldots, L$) after T iterations, we can explicitly define the number of cutting interfaces as

$$C(T) = \sum_{i=1}^{L-1} \lceil c_{i+1} - c_i \rceil, \tag{2.4}$$

since $0 \leq c_i \leq 1$ by construction. Thus, the number of cuts is not a true proxy of mixing as it does not take into account whether or how the color changes on average. Nevertheless, the number of cuts is meaningful because, if reactions and diffusion are added into the cutting and shuffling protocol, then it is expected that having a wide distribution of cuts will lead to fast homogenization of the material [20, 44]. The number of cuts (discontinuities) is also a quantity of interest in abstract mathematical discussion of IETs [45].

To mitigate some of the weakness of $C(T)$ as a measure of mixing, we also use a mixing norm to quantify mixing. Specifically, we define an "L^p norm" of a function $c(X, T)$ as

$$||c||_p(T) = \left(\frac{\int_0^L |c(X,T) - \bar{c}|^p \, \mathrm{d}X}{\int_0^L \mathrm{d}X} \right)^{1/p}, \tag{2.5}$$

where $1 \leq p < \infty$ and

$$\bar{c} = \frac{\int_0^L c(X,T) \, \mathrm{d}X}{\int_0^L \mathrm{d}X} \tag{2.6}$$

is the *average color* of the line segment. Here, X is continuous variable running along the length of the line segment: $0 \leq X \leq L$. For concreteness, when initially constructing the line segment, we assign each subinterval i a color value $(i-1)/(N-1)$ $(i = 1, \ldots, N)$, which is always between 0 and 1. Thus, the mixing norm $||c||_p(T)$ measures how far the segment's color distribution is from the uniform average concentration/color $\bar{c}$, in an appropriately global way. The case of $p = 2$ is of interest as it measures the variance, or root-mean-square deviation, of the color distribution. As discussed by Thiffeault [46, p. 5], "[v]ariance is thus a useful measure of mixing: the smaller the variance, the better the mixing." And, while

the average $\bar{c}$ remains constant in time and unchanged by diffusion for periodic boundary conditions, the variance is depleted as long as there is diffusion and non-zero color gradients along the line segment [46], with the cutting and shuffling process controlling how gradients are created and, thus, the decay rate.

To compute the mixing norm from the discrete data of our cutting and shuffling simulations, consider a distribution of colors $c(X,T)$ across the line segment $0 \leq X \leq L$. After T iterations of cutting and shuffling, c_j represents the color value of the jth continuous-color piece, where $j = 1, \ldots, k(T)$, and $k(T)$ is the number of continuous-color subsegments after T iterations. For example, in Figure 2.1, when $T = 0$, $k(T) = 4$, $c_j = 0, 1/3, 2/3, 1$ for the color "black," "red," "yellow" and "white," respectively. While when $T = 1$, $k(T) = 4$ and $c_1 = 2/3$, $c_2 = 0$, $c_3 = 1$, $c_4 = 1/3$ because the cutting and shuffling process changed the location of the colors. And when $T = 2$, $k(T) = 7$ and $c_j = 0, 1, 2/3, 1, 1/3, 2/3, 0$ shows that the color distribution has become more complex due to mixing. In addition, each l_j is an integer and can be calculated based on the cutting and shuffling algorithm. Then, we can compute the integrals in the definition of the mixing norm exactly over each continuous-color piece and reduce the definition from Equation (2.6) to

$$||c||_p(T) = \left(\frac{\sum_{j=1}^{k(T)} |c_j - \bar{c}|^p l_j}{\sum_{j=1}^{k(T)} l_j} \right)^{1/p}, \tag{2.7}$$

where

$$\bar{c} = \bar{c}(r, N) = \frac{\sum_{j=1}^{N} c_j l_j}{\sum_{j=1}^{N} l_j} \qquad (T = 0) \tag{2.8}$$

is, as before, the uniform average concentration/color of the initial condition. Note that $\sum_{j=1}^{k(T)} l_j = L$ by definition, where L is given by Equation (2.3), and l_j is the length of jth subsegment of continuous color. At iteration T, there are $1 \leq k(T) \leq L$ pieces of continuous color with $k(0) = N$. For $p = 2$, Equation (2.7) describes the standard deviation (square root of the variance) of the mixture. If normalized appropriately, the $p = 2$ mix norm can be made to agree with Dankwerts' classical definition of the *intensity of segregation* [47], which he used to quantify mixing.

2.4 Visualizing Mixing: Space-time and Waterfall Plots

Mixing of a line segment by cutting and shuffling can be visually represented by space-time plots as initially discussed in [19]. To create a space-time plot, we combine all line segments after each iteration and arrange them from bottom to top in a two-dimensional (2D) space-time plot. The horizontal axis is the dimensionless lattice position X/L, while the vertical axis represents the number of iterations T. From space-time plots, we can visually identify the evolution of mixing, including periodic behavior and poor mixing. Figure 2.3(a) shows an example of a space-time plot of a cutting and shuffling protocol.

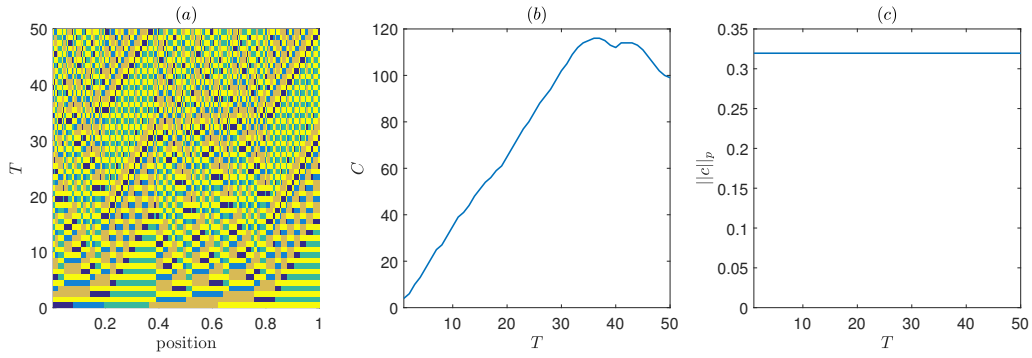

Figure 2.3. Mixing by cutting and shuffling with $N = 5$, $r = 1.5$, $\Pi = [52413]$, $T = 50$. (a) Space-time plot of the color evolution. (b) Growth of the number of cutting interface $C(T)$. (c) Evolution of the mixing norm $\|c\|_p(T)$.

In Figure 2.3(b), we plot the number of cuts $C(T)$, which grows in time but levels out after a while and starts decreasing. This protocol is ultimately periodic, so even over many iterations it does not produce good mixing. In Figure 2.3(c), we plot the mixing norm $\|c\|_p(T)$ for this case. The mixing norm remains constant, meaning that the color distribution never approaches the average color. Of course, since cutting and shuffling merely redistributes the color pieces, without changing their individual colors, the distribution cannot approach the average (see also [39, Section 4]). The latter is, of course, the classical distinction of *stirring* versus *mixing* [4, 48, 49]. That is to say, while cutting and shuffling (the "mechanical"

stirring process in our approach) can significantly disperse the initially continuous color segments, diffusion (such as molecular diffusion in a fluid or collisional diffusion in a granular flow) is needed to ultimately homogenize and mix the material. This distinction and the interplay between stirring and mixing brings us to a key contribution of the present work: incorporating diffusion into IETs and examining the resulting universal mixing behaviors.

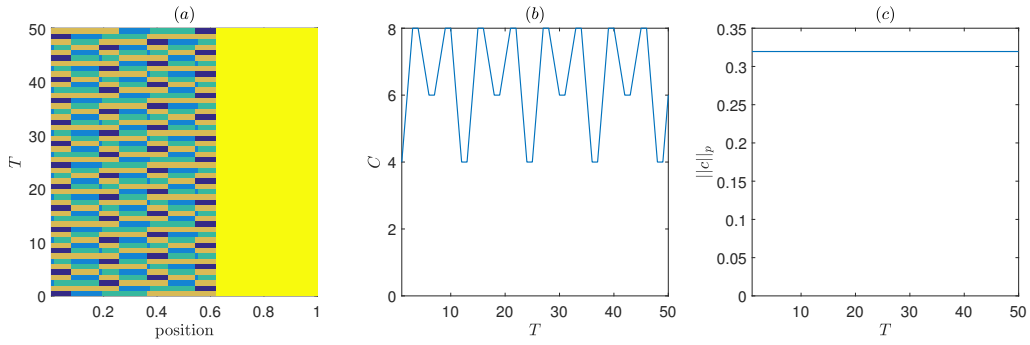

Figure 2.4. Example of mixing with $N = 5, r = 1.5, \Pi = [42315], T_{\max} = 50$.

Figures 2.4 and 2.5 show two additional examples of mixing by cutting and shuffling without diffusion under different permutation (shuffling) protocols. On the one hand, Figure 2.4 shows a case of a permutation that maintains the last subsegment fixed. Therefore, only the first four subsegments are cut and shuffled in this example, thus the cutting interfaces reaches a maximum and begins to follow a periodic pattern after only a few iterations. On the other hand, Figure 2.5 shows an example with the same shuffling permutation as Figure 2.3 but with a different ratio $r = 1.25$. In this case, within the 50 iterations shown, the cutting interfaces has not shown a periodic pattern. Therefore, it should be clear that the ratio r has a nontrivial impact on the dynamics and (potential) periodicity of the number of cutting interfaces.

Another approach to visualize mixing of a line segment by cutting and shuffling can be presented by a three-dimensional (3D) waterfall plot. In MATLAB, we can create a 3D matrix to store the color distribution after multiple cutting and shuffling processes. The matrix can be displayed by the built-in function `waterfall`. One in-plane axis is the rescaled

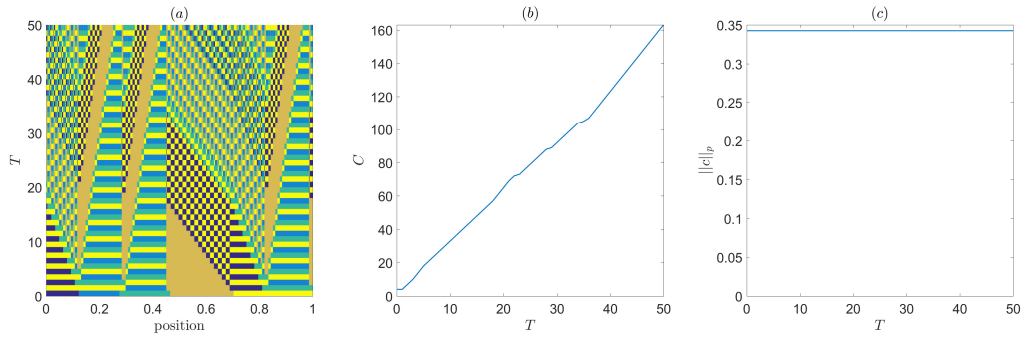

Figure 2.5. Example of mixing with $N = 5, r = 1.25, \Pi = [52413], T_{\max} = 50$.

lattice position X/L as in the space-time plot, the other in-plane axis again represents the number of iterations T, while the vertical axis in the waterfall plot is the color value c as mentioned in Section 2.3. From waterfall plots, we can visualize the change of color values between different lattices and how cutting and shuffling influence the distribution of different colors. Specifically, it is much easier to see the abrupt change of colors due to the step-wise distribution of the initial color values along the subsegment. Figure 2.6 shows an example of a waterfall plot with the same cutting and shuffling protocol as Figure 2.3. For completeness, Figures 2.7 and 2.8 show examples of the waterfall plots with the same cutting and shuffling protocols as Figures 2.4 and 2.5, respectively.

2.5 Incorporating Diffusion

To ensure complete and thorough mixing of a line segment, *i.e.*, $c(X, T) \to \bar{c}$ for all $X \in [0, L]$ as $T \to \infty$, we must incorporate diffusion into the system. As is well known, diffusion by itself would mix an initial line segment (such as the one shown in the top row of Figure 2.1) very slowly. Thus, here we are interested in the *nontrivial* interaction of cutting and shuffling (redistribution of color) and diffusion (relaxation of the color distribution to the mean).

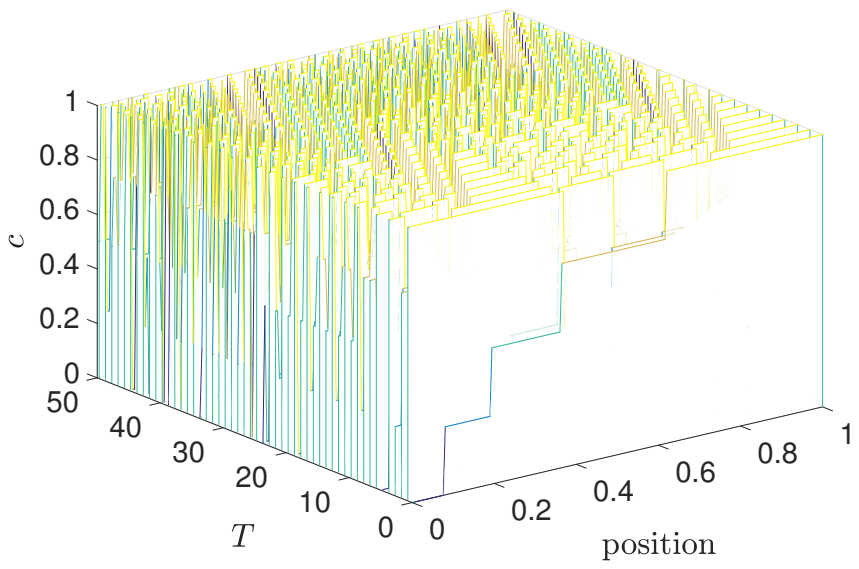

Figure 2.6. Waterfall plot with $N = 5$, $r = 1.5$, $\Pi = [52413]$, $T_{\max} = 50$, corresponding to Figure 2.3(a).

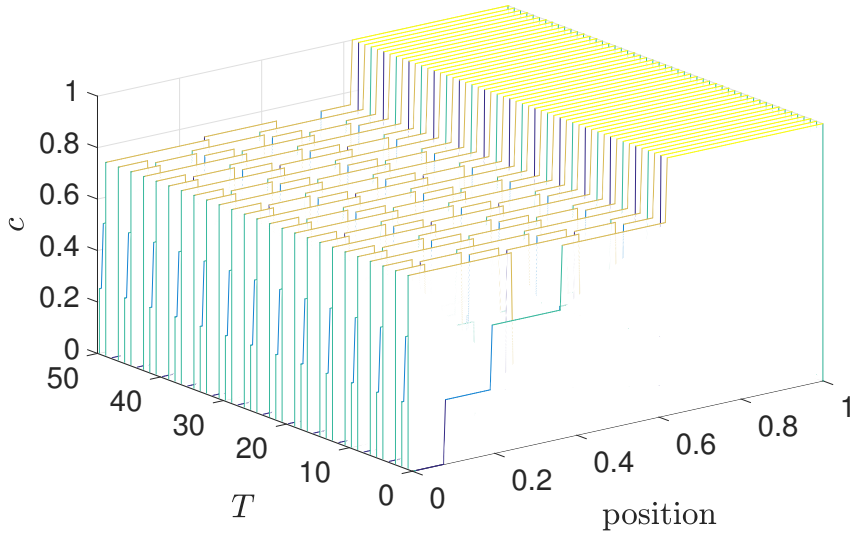

Figure 2.7. Waterfall plot with $N = 5$, $r = 1.5$, $\Pi = [42315]$, $T_{\max} = 50$, corresponding to Figure 2.4(a).

Following Pierrehumbert [50], we would like to incorporate a *time-discrete* diffusion step between cutting and shuffling steps. To this end, consider a generic diffusion equation for the concentration/color $c(X, T)$ with characteristic diffusivity D:

$$\frac{\partial c}{\partial T} = D\frac{\partial^2 c}{\partial X^2}, \tag{2.9}$$

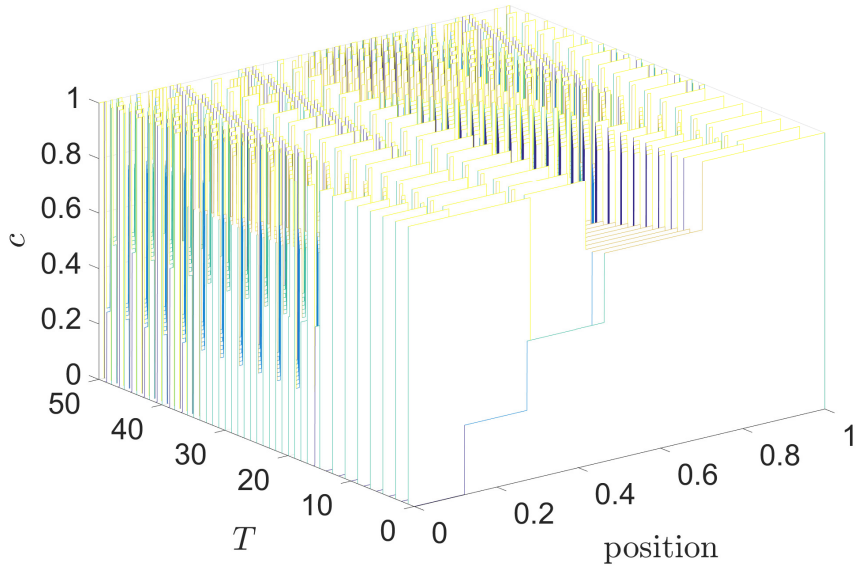

Figure 2.8. Waterfall plot with $N = 5$, $r = 1.25$, $\Pi = [52413]$, $T_{\max} = 50$, corresponding to Figure 2.5(a).

where $X \in [0, L]$ and $T \in [0, T_{\max}]$. We can discretize Equation (2.9) using the usual forward-time, central-space (FTCS) scheme [51]:

$$\frac{c_i^{n+1} - c_i^n}{\Delta T} = D\frac{c_{i+1}^n - 2c_i^n + c_{i-1}^n}{(\Delta X)^2}, \tag{2.10}$$

where $c_i^n \approx c(X_i, T^n)$ with $X_i = i\Delta X$ and $T^n = n\Delta T$. This discretization is stable if $D\Delta T \leq \frac{1}{2}(\Delta X)^2$.

However, in our cutting and shuffling protocols, the color is only defined on integer lattice points, and we iterate by integer increments in time, *i.e.*, $\Delta X = \Delta T = 1$. Then, given the standard stability criterion for the scheme in Equation (2.10), we must restrict our equivalent diffusion coefficient such that $D \leq 1/2$.

Therefore, diffusion can be incorporated into cutting and shuffling by an additional sweep through the lattice at each iteration of the IET. That is to say, after the line segment is cut and shuffled as described above, an additional sweep through the lattice points is performed using the replacement rule:

$$c_i \mapsto (1 - 2D)c_i + Dc_{i+1} + Dc_{i-1}, \tag{2.11}$$

where c_i is the color value at the ith lattice point ($i = 1, 2, \ldots, L$). A common choice is $D = 1/2$, in which case our replacement rule from Equation (2.11) becomes a simple averaging: $c_i \mapsto \frac{1}{2}(c_{i+1} + c_{i-1})$. Given a particular diffusion coefficient D, we would like to show that the line segment can be completely mixed in much fewer iterations than by the IET alone. To completely specify the diffusion rule, periodic boundary conditions are used to set $c_{L+1} = c_1$ and $c_0 = c_L$.

We would like all of our simulations to have the same "effective" diffusion coefficient, D, as it might arise from inter-particle collisions in a granular medium (see, *e.g.*, [52]). However, the length L of the lattice depends on N and r as discussed in Section 2.2, see Table 2.1. Hence, a fixed diffusion coefficient does not yield the same behavior on different lattices, over the same number of iterations, simply because of the change in the line segment's length. To ensure an "equivalent" diffusion behavior across lattices of different L, we apply dimensional analysis to connect the number of iterations that a given IET is required to run for, given a fixed diffusivity D but different domain lengths. The problem reduces to matching dimensionless diffusion coefficients once the domain is mapped from $[0, L]$ to $[0, 1]$ and the number of iterations (from 0 to T) is normalized to a discrete time-like variable running from 0 to 1.

To this end, consider two cases of cutting and shuffling protocols with diffusion, the first with D_1, $T_{\max,1}$ and L_1 and the second with D_2, $T_{\max,2}$ and L_2. From dimensional analysis, we should ensure that the dimensionless diffusion coefficients (*i.e.*, the inverse Péclet numbers assuming the intrinsic velocity scale L/T) match:

$$\frac{D_2 T_{\max,2}}{L_2^2} = \frac{D_1 T_{\max,1}}{L_1^2}. \tag{2.12}$$

Assuming equal diffusivity ($D_1 = D_2$), the diffusion coefficient cancels out, and we can relate the number of iterations $T_{\max,2}$ needed on a lattice of length L_2 to those ($T_{\max,1}$ and L_1) of the reference lattice:

$$T_{\max,2} = \left(\frac{L_2}{L_1}\right)^2 T_{\max,1}. \tag{2.13}$$

To illustrate the importance of using dimensional analysis, specifically Equation (2.13) to match the number of iterations of different cutting and shuffling protocols, Figure 2.9 shows

Table 2.1. Dependence of L on r, here specifically for $N = 4$, and the corresponding variation in the number of iterations, via Equation (2.13), with the first row ($r = 1.25$ and $T_{\max} = 50$) being the reference system for the remaining.

r	r_n	ξ	L	$T_{\max}$
1.25	5	64	369	50
1.2	6	125	671	166
1.4	7	125	888	290
1.6	8	125	1157	492
1.8	9	125	1484	809
1.1	11	1000	4641	7910
1.3	13	1000	6187	14057

the decay of the mixing norm for three different values of r, (a) without normalizing the number of iterations using $T_{\max}$ and (b) after properly normalizing the number of iterations using dimensional analysis. In other words, in Figure 2.9(a), we did not use dimensional analysis and fixed the maximum number of iterations to 50. Then, it is clearly seen that because different r correspond to different L, the mixing behavior is incommensurately different in the three cases, so no conclusions can be drawn from Figure 2.9(a). On the other hand, in Figure 2.9(b), we used dimensional analysis to properly match $T_{\max}$ across different r (and, thus, L). The result is that, when the ratio r is more "complex," the mixing norm should decrease much faster because mixing is enhanced for these cases as argued in [19, 22]. This behavior is now clearly observed in Figure 2.9(b). Thus, Figure 2.9 clearly illustrates the importance of dimensional analysis when incorporating diffusion into cutting and shuffling, and the significance of Equation (2.13).

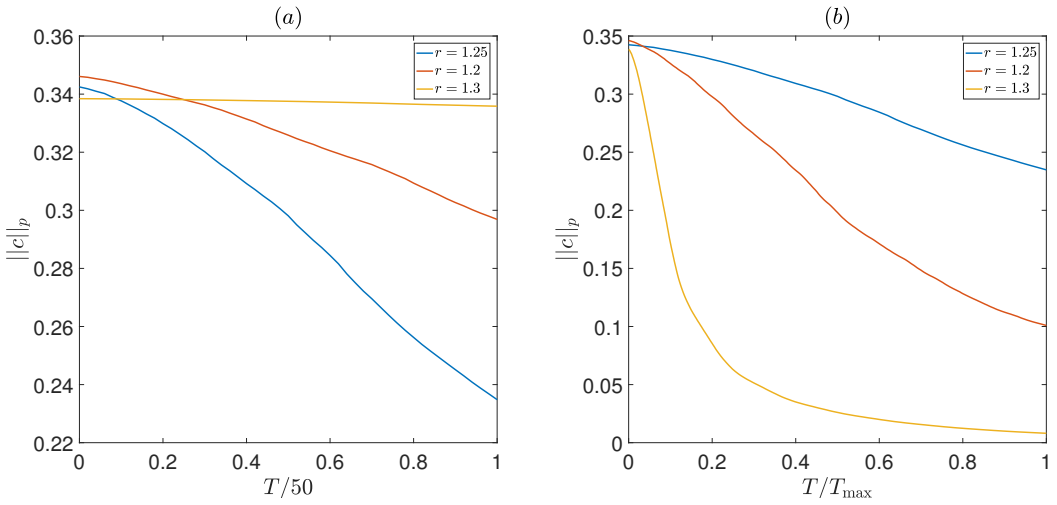

Figure 2.9. Decay of the mixing norm for fixed $N = 5$, $\Pi = [52413]$, $D = 0.5$, and three choices of the segment ratio r. In (a), all three cases are ran for the same 50 iterations, showing incomparable behaviors. In (b), the maximum number of iterations is properly match via Equation (2.13), allowing a comparison across the three protocols.

3. RESULTS AND DISCUSSION

In this chapter, we examine the mixing outcomes of cutting and shuffling in the presence of diffusion. Specifically, we address the hypothesis that cut-offs and universal behavior exists in the family of IETs with diffusion that we have described/constructed above. In Section 3.1, after defining how to incorporate diffusion into the system, we compare cases with "large" and "small" diffusivity. In Section 3.2, a fit function of cutting interfaces was introduced to quantify the degree of mixing. The fitting parameters of different systems are compared. In Section 3.3, the mixing norm can also be fitted into an exponential function. The relationship between system parameters and fitting parameters is also clarified. In Section 3.4, a universal mixing behavior was discovered among different systems after we introduce the half-mixing time T_{Pe}. In Section 3.5, we tried to predict the stopping time T_{Pe} and verified with the *average* subsegment length.

Previous work has sufficiently addressed the non-diffusive (*i.e.*, deterministic) mixing by IETs both mathematically and through simulation studies. Therefore, in this subsection, we summarize just the key results. From [19, 22], it is clear that the number of subsegments N, the permutation Π and the ratio r greatly affect the mixing outcomes. Specifically, three "design rules" have been suggested to improve the mixing behavior (recall the discussion in Section 2.2):

(i) Reducible and rotational permutations, as well as those that exhibit unsatisfactory shuffling, should be excluded.

(ii) The line segment should be cut into no more than six subsegments (*i.e.*, $N \leq 6$), larger N do not significantly improve mixing.

(iii) The ratio r should not be "large," *i.e.*, it should ideally be an irrational number close to 1. (Continued fraction expansions can be used to quantify "how irrational" r is.)

3.1 Mixing Behavior of IETs with Diffusion

In the present work, motivated by the hypothesis that IETs with diffusion exhibit cut-offs in the sense of card shuffling, we are first interested in establishing how the mixing behaviors previously studied are affected by the presence of diffusion. Specifically, we study the effect of the diffusion coefficient's magnitude (*e.g.*, $D = 0, 0.01, 0.5, \ldots$), having matched the total iterations T using the dimensional analysis rules from Section 2.5 to ensure comparable "amounts" of diffusion across lattices of different lengths.

As an introductory example, let us consider how a typical space-time plot, such as the one shown in Figure 2.3(a) changes when diffusivity with $D = 0.5$ is incorporated into the cutting and shuffling process. Under the same parameters as Figure 2.3(a), Figure 3.1(a) shows the space-time plot of mixing by cutting and shuffling including diffusion. The most obvious effect is that the space-time plot becomes "fuzzy" as diffusion now blurs the different colors of the subsegments being cut and shuffled about. Figure 3.2 also shows the distribution of different color value after incorporating diffusion, in the form of a waterfall plot. We can see that the difference between distinct colors is vanishing, and the value of colors is becoming more uniform with increasing T.

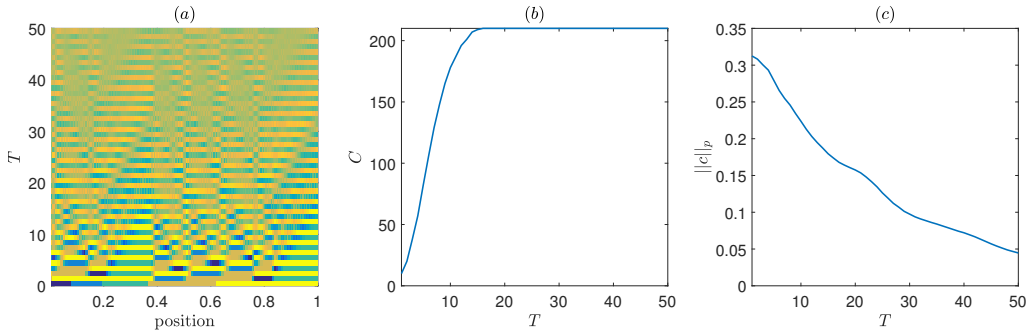

Figure 3.1. Incorporating diffusion with $D = 0.5$ into the IET from Figure 2.3 with $N = 5$, $r = 1.5$, $\Pi = [52413]$, and $T_{\max} = 50$.

We can also examine how the number of cutting interfaces $C(T)$ and the mixing norm $\|c\|_p(T)$ evolve in the presence of diffusion. Compared with Figure 2.3(b), the number of

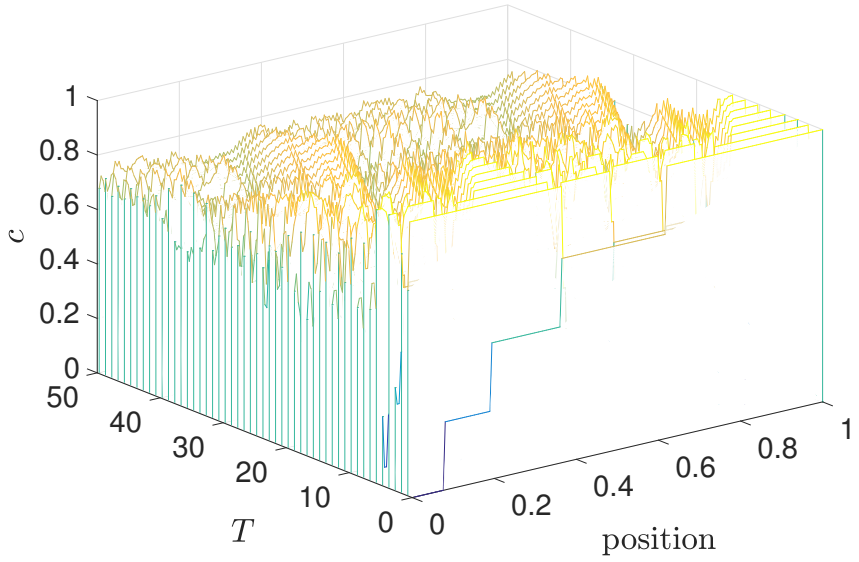

Figure 3.2. Waterfall plot with $N = 5$, $r = 1.5$, $\Pi = [52413]$, $T_{\max} = 50$, $D = 0.5$, corresponding to Figure 3.1(a).

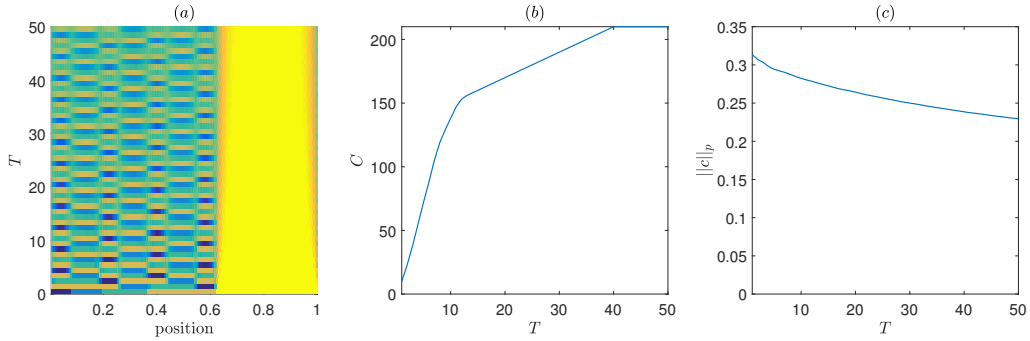

Figure 3.3. Incorporating diffusion with $D = 0.5$ with $N = 5, r = 1.5, \Pi = [42315], T_{\max} = 50$, corresponding to Figure 2.4.

cutting interfaces in Figure 3.1(b) grows quickly and reaches an absolute maximum. This difference in how $C(T)$ evolves is due to the fact that material is now not just cut and shuffled but also mixed by diffusion. Diffusion changes the color of nearby lattice points through the diffusion rule [given by Equation (2.11)], thereby quickly causing nearby lattice points to have slightly different color values. In a small number of iterations, the number

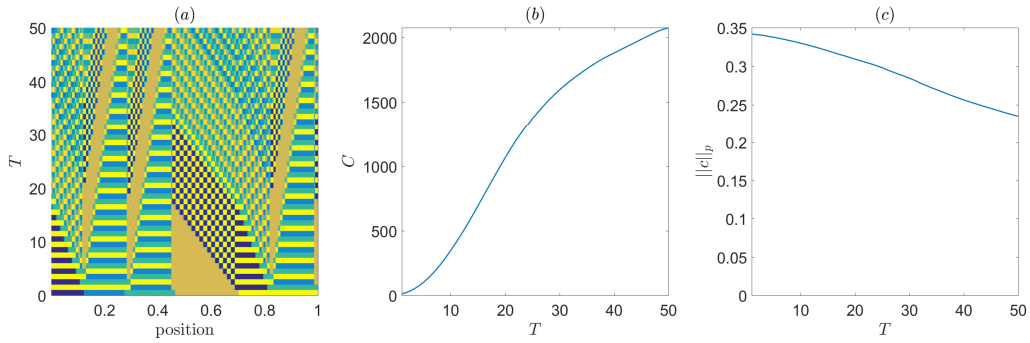

Figure 3.4. Incorporating diffusion with $D = 0.5$ with $N = 5, r = 1.25, \Pi = [52413], T_{\max} = 50$, corresponding to Figure 2.5.

of cutting interfaces $C(T)$ increases without exhibiting periodic patterns, and reaches its absolute maximum value $\max_T C(T) = L - 1$. This upper bound is due to the fact that eventually the color of *every* lattice is distinct from every other (even if just slightly so) due to cutting, shuffling and diffusion.

The mixing norm $||c||_p(T)$, on the other hand, now decreases (asymptotically to 0) with T, as seen in Figure 3.1(c), instead of remaining constant as in Figure 2.3(c). In the presence of diffusion, the cutting and shuffling process eventually drives the color of the line segment to the average one, $\bar{c}$, which is set by the initial conditions. Figures 3.3 and 3.4 also show the effect of incorporating diffusion but for the protocols shown (without diffusion) in Figures 2.4 and 2.5, respectively. As in Figure 3.1, the number of cutting interfaces continues to grow with T, while the mixing norm decays.

Next, we would like to establish the effect of varying the diffusion coefficient D (*i.e.*, "small" diffusivity versus "large" diffusivity). For smaller diffusion coefficient $D = 0.01$, the mixing behavior is shown in Figure 3.5. The growth of cutting interfaces $C(T)$ in Figure 3.1(b) is almost the same as in Figure 3.5(b), showing a weak sensitivity to the diffusivity [1]. And Figure 3.6 shows the waterfall plot corresponding to Figure 3.5. This

[1]In our definition of $C(T)$, *i.e.*, Equation (2.4), any slight change in the color of nearby lattice points is counted as a cut. We use this definition so that $C(T)$ can be generalized to the case with diffusion considered herein.

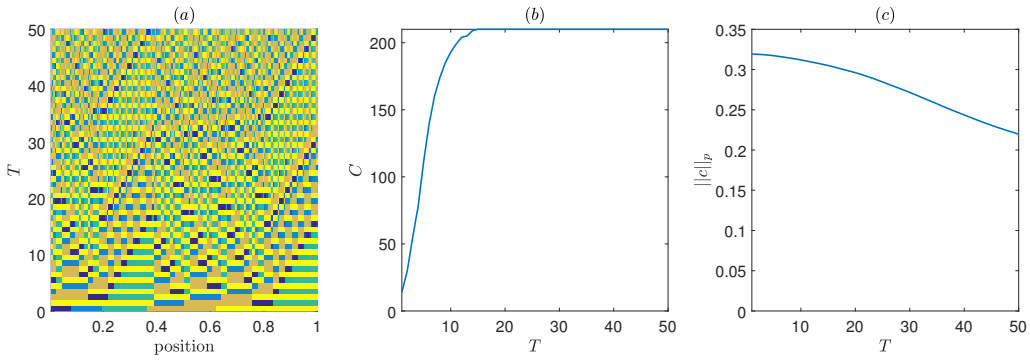

Figure 3.5. Incorporating "small" diffusion with $D = 0.01$ into the IET from Figure 2.3 with $N = 5$, $r = 1.5$, $\Pi = [52413]$, and $T_{\max} = 50$, corresponding to Figure 2.3.

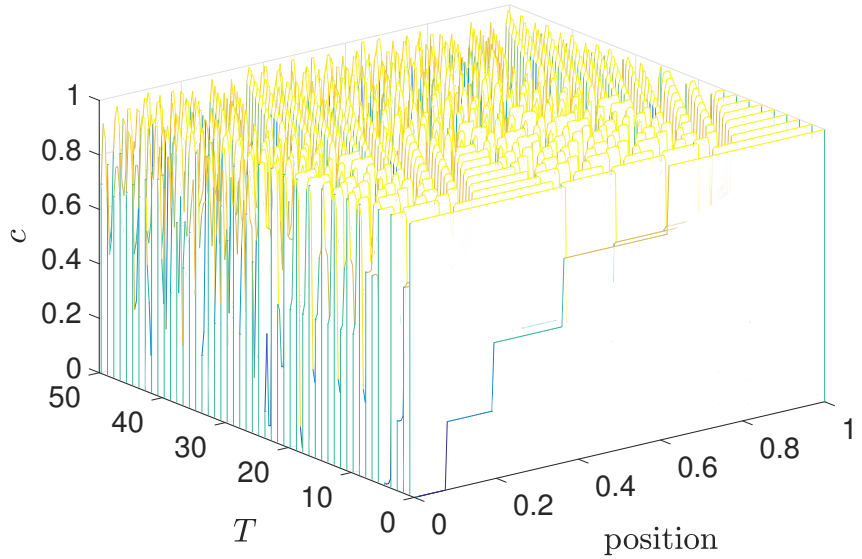

Figure 3.6. Waterfall plot with $N = 5$, $r = 1.5$, $\Pi = [52413]$, $T_{\max} = 50$, $D = 0.01$, corresponding to Figure 3.5(a).

observation suggest that $C(T)$ might not be an effective way to measure the degree of mixing among systems with different diffusion coefficients. While in the deterministic (no diffusion) case, insightful mathematical results can be obtained about the growth of the number of cuts [45], any amount of diffusion perturbs the color values so that differences

in color that are counted as "cuts" appear immediately. Although one can invent threshold criteria for how much change $|c_i - c_{i+1}|$ should signal a "cut," this is ultimately a fruitless task. Meanwhile the mixing norm $\|c\|_p(T)$ in Figure 3.5(c) decays much more slowly that in Figure 3.1(c), showing (as is to be expected on the basis of previous studies, *e.g.*, [37–40]) that the mixing norm effectively quantifies the differences in the mixing process with "small" diffusion ($D = 0.01$) versus "large" diffusion ($D = 0.5$). Figure 3.6 also shows the waterfall plot of color distribution for a small diffusivity ($D = 0.01$), which is quite similar with the no diffusion case.

3.2 Quantifying the Evolution of the Number of Cutting Interfaces

Based on the numerical evidence in Figures 3.1(b) and 3.5(b), we suggest that the evolution of $C(T)$ can be approximated by a parametrization involving the "error function":

$$C(T) \simeq (2a - b) + (b - a) \left\{ 1 + \operatorname{erf} \left[\left(\frac{T}{\tau} \right)^{\alpha} \right] \right\} \left(\tag{3.1}$$

where $a = \min_T C(T) = C(0)$ and $b = \max_T C(T) = L - 1$, but τ and α are *a priori* unknown fitting parameter. For a fixed ratio r and number of subsegments N, we average the $C(T)$ curves across different permutations and fit the averaged curve to Equation (3.1), providing the values of τ and α tabulated in Table 3.1. Figure 3.7 shows an example of this procedure, the gray curves represent $C(T)$ for the different permutations considered, while the red curve is the average value of $C(T)$ across permutations, and the blue dashed line is the curve according to Equation (3.1). We observe that the proposed fit function captures the overall trend of the average number of cuts quite well.

The second step is to vary the diffusion coefficient D and subsegment length ratio r, and Figure 3.8 shows the fit curve of the average for a range of r and D values. The more complex r is, the less time it takes to reach complete mixing. And generally a larger diffusion coefficient ($D = 0.5$) takes less time to reach complete mixing compared with a smaller one ($D = 0.01$). Table 3.1 summarizes the fitting parameters among all these different systems. The constant τ becomes smaller when the system reaches complete mixing earlier. Therefore,

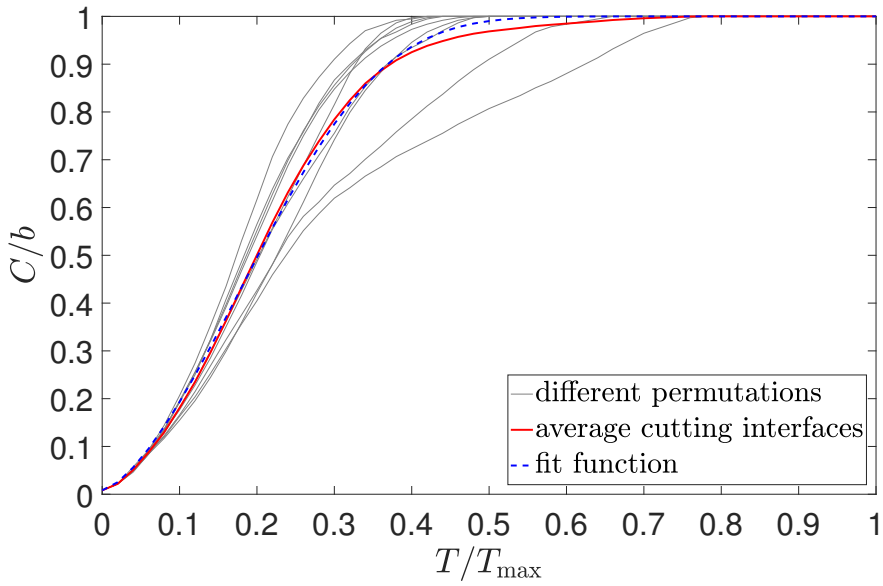

Figure 3.7. Fit $C(T)$ with $T_{\max} = 50$, $r = 1.25$, $N = 4$, $D = 0.5$, $a = 3$, $b = 368$, the fitting parameters are $\tau = 0.3335$, $\alpha = 1.4866$.

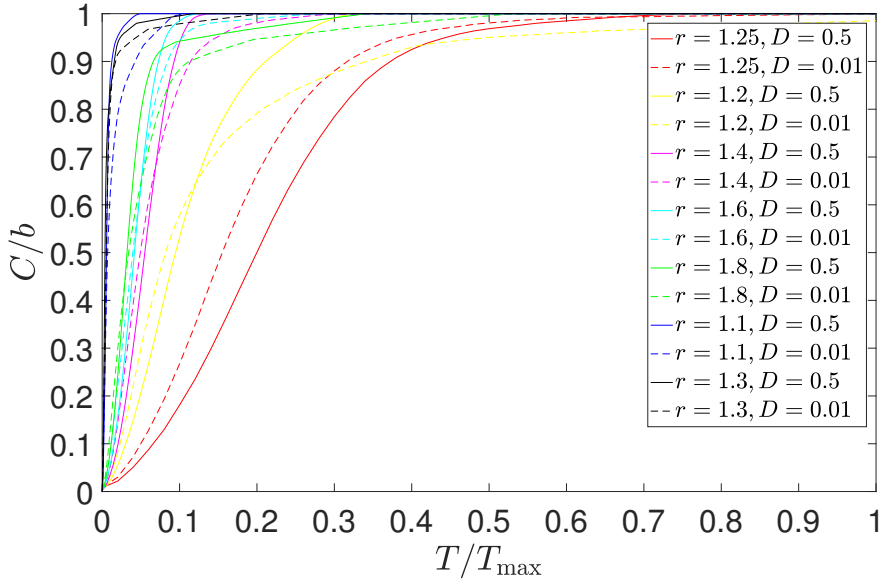

Figure 3.8. Different average $C(T)$ fit curves, such as the specific one shown in Figure 3.7, but as r and D are varied with $N = 4$.

Table 3.1. Fitting parameters τ and α of $C(T)$ $(N = 4)$ according to the model in Equation (3.1), for different choices of r and D.

	$D = 0.5$		$D = 0.01$	
r	τ	α	τ	α
1.25	0.3335	1.4866	0.2760	1.3503
1.2	0.1782	1.2422	0.2573	0.6941
1.4	0.0848	1.7301	0.0981	1.1428
1.6	0.0657	1.6464	0.0735	1.2172
1.8	0.0571	1.3389	0.0939	0.7574
1.1	0.0101	1.2957	0.0287	0.5576
1.3	0.0109	0.7208	0.0137	0.7440

we understand τ as a time constant (with units of numbers of iterations), which characterizes the speed of mixing in the system.

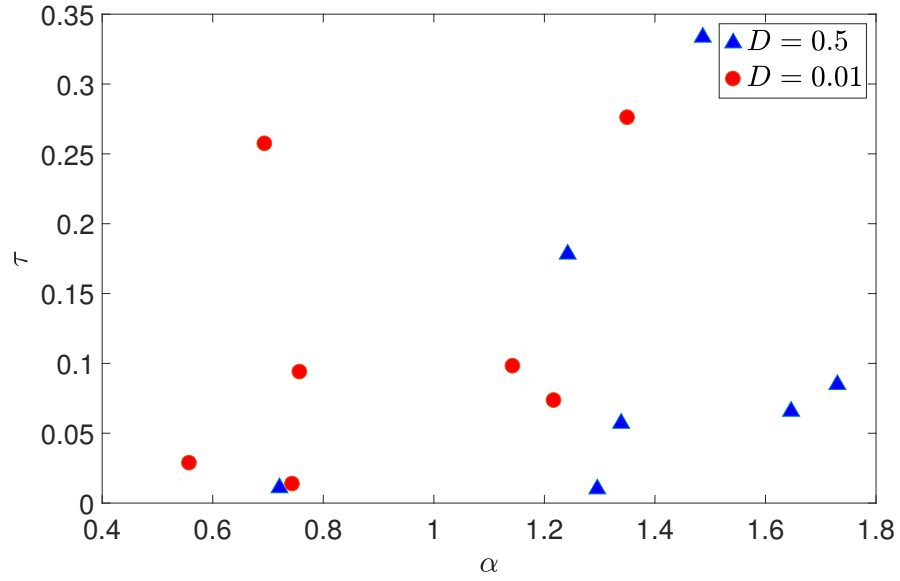

Figure 3.9. Scatter plot in the (α, τ) plane of $C(T)$ from Figure 3.8 (see also Table 3.1).

Figure 3.9 shows the scatter plot of τ and α values. This figure and approach to analyzing our data is inspired by the so-called τ-*bias* scatter plots of McIlhany and Wiggins [53]. In [53], the normalized variance of concentration was used to quantify the degree of fluid mixing in a microfluidic device. The parameters τ and *bias* were introduced to quantify the evolution of concentration variance curve and, thus, mixing. The parameter τ is, just as in the present work, interpreted as a time constant describing the temporal decay of the variance of concentration, while *bias* quantifies the "unmixedness" of the final asymptotic state. For our analysis of the $C(T)$ curves, the concept of *bias* is not applicable, so instead we have the skewness parameter α, in addition to τ.

The best cases are on the bottom of the Figure 3.9, since the time constant τ is relatively small, which means the mixing process is completed quickly. In these cases, the subsegment ratio r is, for example, $r = 1.1$ and 1.3. The worst cases are on the top of Figure 3.9, which have large time constants. Comparing cases with the same ratio r and different diffusivity

D, we see that when D is quite small ($D = 0.01$), it usually takes longer for the system to mix (larger τ).

3.3 Quantifying the Effect of Diffusion on the Decay of the Mixing Norm

Based on the numerical evidence in Figures 3.1(c) and 3.5(c), we suggest that the evolution of $||c||_p(T)$ can be approximated by a *stretched-exponential* function:[2]

$$||c||_p(T) \simeq M \cdot e^{-(T/\tau)^\alpha}, \tag{3.2}$$

where $M = ||c||_p(0)$ is the initial norm before mixing but τ and α are *a priori* unknown fitting parameters. The time constant τ quantifies how fast the mixing norm decays with T, while α determines how skewed the decay curve is. If $\alpha = 1$, the fit function in Equation (3.2) is a "perfect" exponential, while for $\alpha < 1$, it is skewed and decays more slowly (asymptotically as $T \to \infty$).

For a fixed ratio r and number of subsegments N, we average the mixing norm evolution curve $||c||_p(T)$ across different permutations as shown in Figure 3.10, then we fit the averaged profile to Equation (3.2). MATLAB's nonlinear least-squares subroutine is used to obtain the best-fit values of the parameters. This procedure provides the numerical values of τ and α. We use the same approach to obtain the curves of averaged mixing norm, which are shown in Figure 3.11, as r and D are varied. Table 3.2 tabulates the values of τ and α for the different cutting and shuffling systems considered in Figures 3.10 and 3.11.

Figure 3.10 shows an example of this procedure, the gray curves represent $||c||_p(T)$ for the different permutations Π considered, while the red curve is the average value of $||c||_p(T)$ across permutations, and the blue dashed line is the fit curve according to Equation (3.2). We observe that the proposed fit function captures the overall trend of the decay of the mixing norm's average across permutations quite well.

The second step is to vary the diffusion coefficient D and subsegment length ratio r, plotting the fit curves of the average in Figure 3.11. The more "complex" r is (see, *e.g.*, the

[2]The choice of a stretched-exponential function is based on the fact that such a parametrization arises and accurately describes a wide range of relaxation processes in disordered condensed matter systems [54].

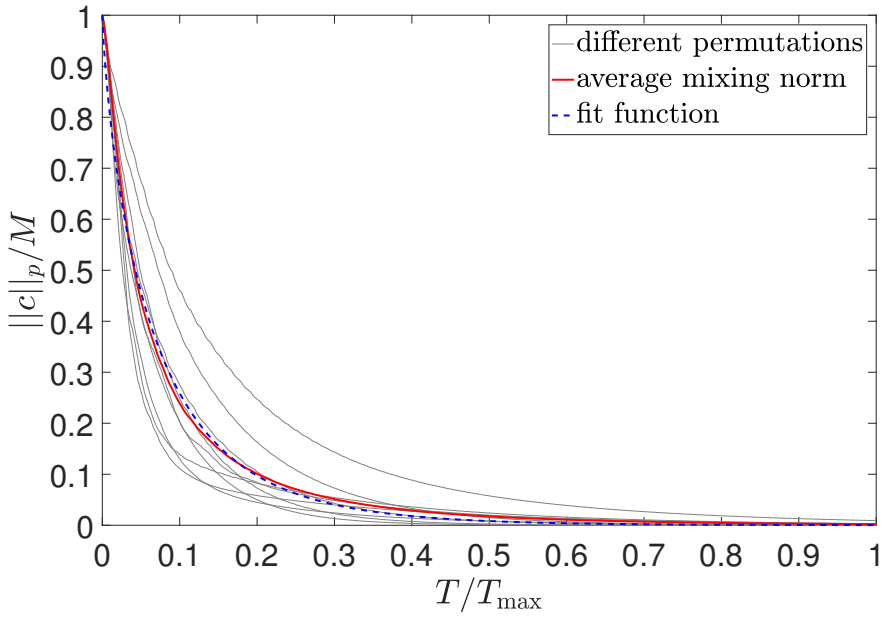

Figure 3.10. Mixing norm decay curves $||c||_p(T)$ with $N = 4$, $r = 1.25$, $M = 0.3650$, $D = 0.5$ and $T_{\max} = 1000$ iterations for various Π (as chosen according to the rules in Section 2.2), shown as gray curves. The average mixing norm decay curve is shown in red, and its fit in dashed blue. The best-fit parameters, according to Equation (3.2), for the average curve are $\tau = 0.0682$ and $\alpha = 0.7866$.

Table 3.2. Fitting parameters of $||c||_p(T)$ according to the model in Equation (3.2) for the *average* mixing norm decay curves shown in Figure 3.11.

	$D = 0.5$		$D = 0.01$	
r	τ	α	τ	α
1.25	0.0682	0.7866	0.3333	0.6471
1.2	0.0397	0.8118	0.1411	0.6385
1.4	0.0203	0.7772	0.1226	0.6660
1.6	0.0128	0.8526	0.0732	0.6794
1.8	0.0137	0.7708	0.0604	0.6017

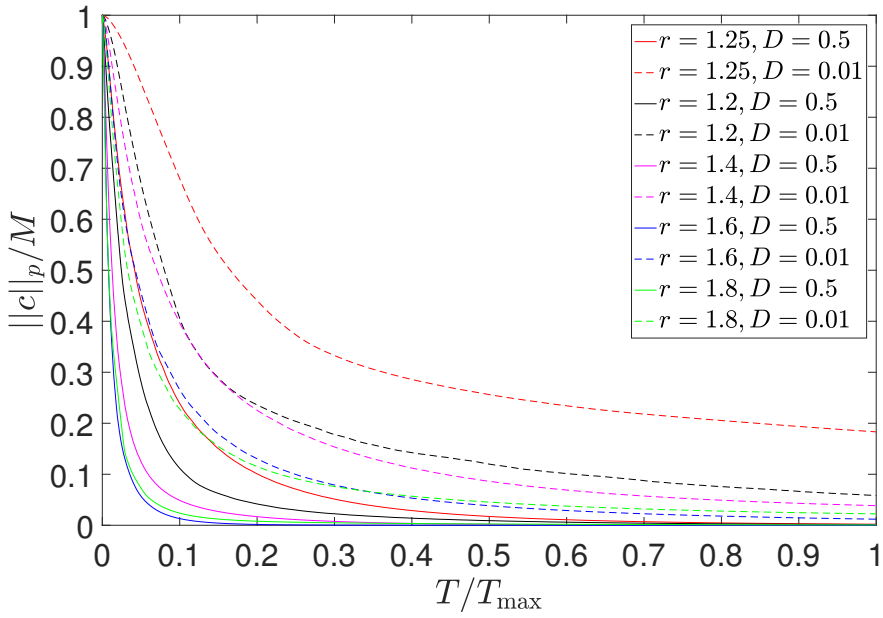

Figure 3.11. The average (across permutations) mixing norm $||c||_p(T)$ decay curve from Figure 3.10 as D (dashed for $D = 0.01$ and solid for $D = 0.5$) and r (different colors) are varied.

discussion in [19] about defining r as a continued-fraction expansion of increasing length), the less time it takes to reach complete mixing. Generally, though there are exceptions, as a careful examination of Figure 3.11 revels. Nevertheless, it takes less iterations to homogenize the line segment with a larger diffusion coefficient ($D = 0.5$) than with a smaller diffusion coefficient ($D = 0.01$), as expected. As discussed above, the connection between the value of r and the resulting cutting and shuffling behavior is highly nontrivial. Thus, our approach of computing the average mixing curve (over all permutations considered) and fitting it via two parameters provides a clear and quantitative way to compare different systems with different r and D. From the values of the fitting parameters summarized in Table 3.2, we infer that the time constant τ is smaller for systems that reach complete mixing in fewer iterations, as expected. Thus, amongst the five choices of r considered,

$$r = 1.6 = 1 + \frac{1}{1 + \frac{1}{1+\frac{1}{2}}} \tag{3.3}$$

results in the swiftest mixing (smallest time constant τ).

Ashwin *et al.* [37] suggested that, in the mixing process, we would like to know how many iterations are required to reach 95% mixing. Thus, we introduce $T_{95\%}$ as the solution to

$$||c||_2(T_{95\%}) \leq 0.05\bar{c}. \tag{3.4}$$

This last equation is easy to solve using our fit function from Equation (3.2),

$$M \cdot e^{-(T_{95\%}/\tau)^{\alpha}} = 0.05\bar{c}. \tag{3.5}$$

Hence,

$$T_{95\%} = \frac{\tau}{\alpha} \ln\left(\frac{M}{0.05\bar{c}}\right)\Bigg(\tag{3.6}$$

where the average concentration $\bar{c}$ depends on r and N as given in Equation (2.8), while some values for τ and α are given in Table 3.2.

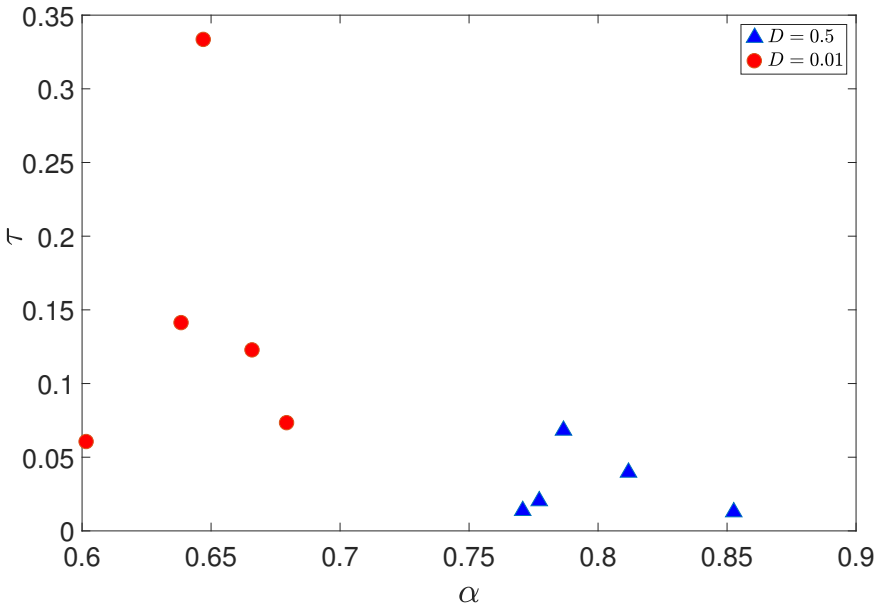

Figure 3.12. Scatter plot in the (α, τ) plane of the fit constants for the mixing norm decay curves from Figure 3.11 (see also Table 3.2). "Good" mixing is observed near the bottom-right corner of the scatter plot, while "poor" mixing is observed near the top-left corner.

Finally, Figure 3.12 shows again the scatter plot of τ and α values based on the idea from [53]. In this work, $bias = 0$ in all cases because the cutting and shuffling process with

diffusion leads to $c_i \to \bar{c}$ for every lattice site i as $T \to \infty$. In [53], it was suggested that small values of *both* τ and *bias* correspond to "good" mixing cases. For our problem, the best mixing case is on the bottom right side of Figure 3.12, which corresponds a small τ but α closer to 1 (*i.e.*, not small). The worst mixing case is on the top left side of the scatter plot, which corresponds to large τ and α significantly different from 1. Therefore, under this interpretation we have a direct relationship between fitting parameters and mixing behaviors. The time constant τ depends most strongly on the ratio r, while α depends most strongly on the diffusion coefficient D, as can be seen from Table 3.2.

3.4 Universal Mixing Curves and Cut-offs

So far, we have shown (a) how to incorporate diffusion into the mixing of a line segment by cutting and shuffling and (b) how quantify mixing across families of protocols via the number of cutting interfaces and the mixing norm. In this section, we would like to substantiate, through numerical results, the central hypothesis of this work: namely that "cut-offs" (and the associated concept of a "stopping times") exists in IETs with diffusion and, furthermore, all mixing behaviors exhibited by cutting and shuffling with diffusion are, in a sense, *universal*. Guided by the work in [27,29,33], we now turn our attention collapsing the mixing norm decay curves of different IETs with diffusion onto a universal profile. As Liang and West [33] note, "[t]o prove the existence of a cutoff is in general very hard, relying on special features of the sequence of systems," thus, for the present purposes, we also settle for numerical evidence thereof.

To this end, let us first consider the number of iterations, denoted by T_{Pe}, required to decrease the initial value of the mixing norm by 50%:

$$||c||_p(T_{Pe}) \approx 0.5||c||_p(0) = 0.5M. \tag{3.7}$$

In the literature on finite Markov chains, the number of iterations T_{Pe} would be called the *stopping time*. In other words, this is the time-to-half-mixing, and the $Pe = DT/L^2$ (recall Section 2.5) subscript reminds us that this number depends on the relative "strength" of diffusion in the problem.

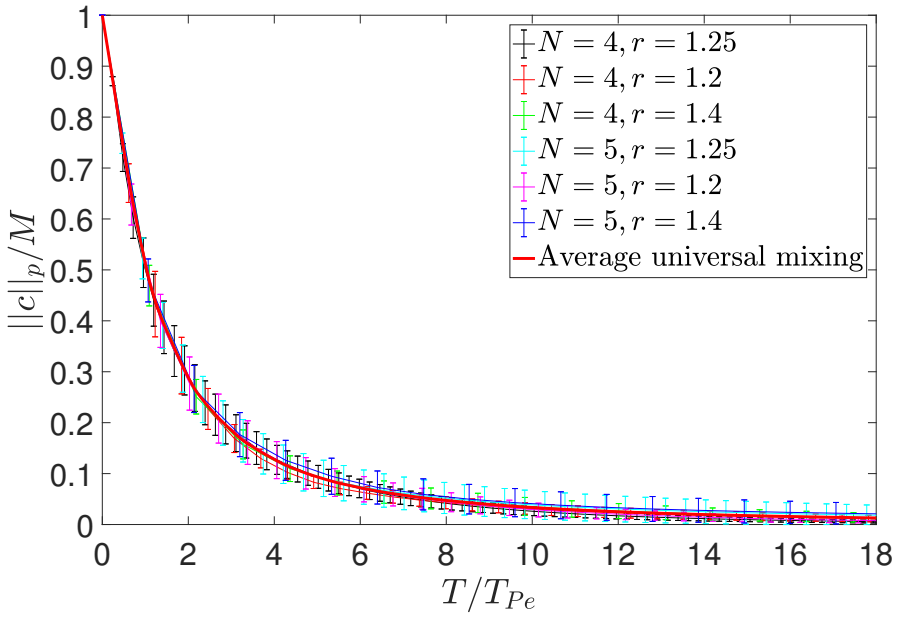

Figure 3.13. Rescaled mixing norm of the concentration/color versus the rescaled iterations, for a diffusion coefficient of $D = 0.5$. A cut-off emerges as all curves collapse, passing through $||c||_p(T)/M = 0.5$ at $T/T_{Pe} = 1$; $p = 2$. The fitting parameters of the average "universal" mixing curve are $\tau_{\text{universal}} = 1.6706$ and $\alpha_{\text{universal}} = 0.7938$.

Next, we rescale each *averaged* mixing norm decay curve (recall Section 3.3) as $||c||_p(T) \mapsto ||c||_p(T)/M$ so that the mixing norm will range from 0 to 1; and, we rescale $T \mapsto T/T_{Pe}$. Then, we plot $||c||_p(T)/M$ versus T/T_{Pe}, for *all* simulations that we have performed, onto the single plot shown in Figure 3.13. A clear collapse of all the data is observed, with all curves passing through $||c||_p(T)/M = 0.5$ at $T/T_{Pe} = 1$, which is the stopping time, as defined in [33]. In this plot, error bars denote one standard deviation from the mean (errors bars are bounded by 0 from below, obviously) of all the concentration curves over all permutations that we have considered. Error bars are used in order to be able to provide a sense for the behavior of all the possible (*i.e.*, across the allowed permutations Π) mixing norm decay profiles in a single plot. Here, each curve corresponds to a given IET with a fixed diffusion coefficient D, segment ratio r and number of pieces N. The most enticing aspect of Figure 3.13 is that a *single universal* profile of the form given in Equation (3.2)

can be fit to the average of all the average curves. It can be calculated that this profile has $\tau_{\text{universal}} = 1.6706$, $\alpha_{\text{universal}} = 0.7938$ (for the chosen $D = 0.5$), which are now independent of N and r (unlike Table 2.1 and Figure 3.11)!

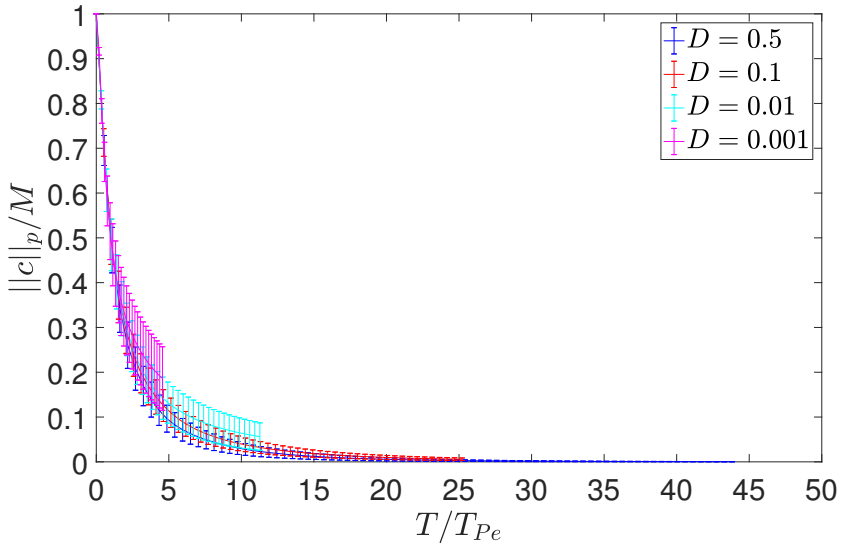

Figure 3.14. Rescaled mixing norm of the concentration/color versus the rescaled iterations, with fixed $N = 5$, $r = 1.2$, $T_{\max} = 2000$ and considering ever smaller diffusivities $D = 0.5, 0.1, 0.01, 0.001$.

In Figure 3.14 we use the same approach to get the value of T_{Pe} and rescale the system. In this case, we consider the average mixing norm with fixed $N = 5$, $r = 1.2$, $T_{\max} = 2000$ but take into consideration different diffusion coefficients, specifically $D = 0.001$, 0.01, 0.1, 0.5. In Figure 3.15, we show a zoom of Figure 3.14 for smaller values of T/T_{Pe} on the horizontal axis. From these two figures, we observe that when the diffusivity is relatively large ($D = 0.01$, 0.1, 0.5), the averaged mixing norm behavior is similar across the choices of D. However, when the diffusivity is quite small (*e.g.*, $D = 0.001$), the mixing norm starts to have the tendency of staying approximately constant (at least for a large initial number of iterations), which leads to the very large error bars on the purple curves. Eventually for $D = 0$, the mixing norm does not change at all with T, hence as $D \to 0$, the error bars must fill the entire plot.

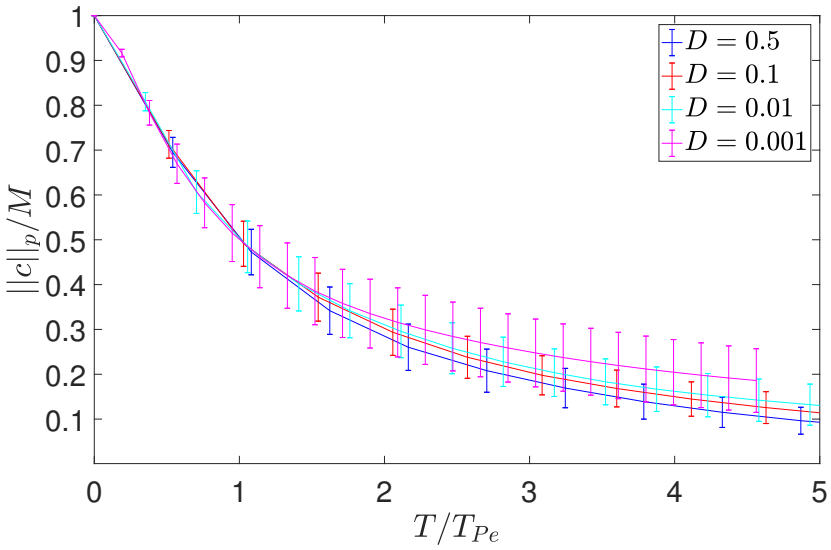

Figure 3.15. Zoom of Figure 3.14 for small values of T/T_{Pe}.

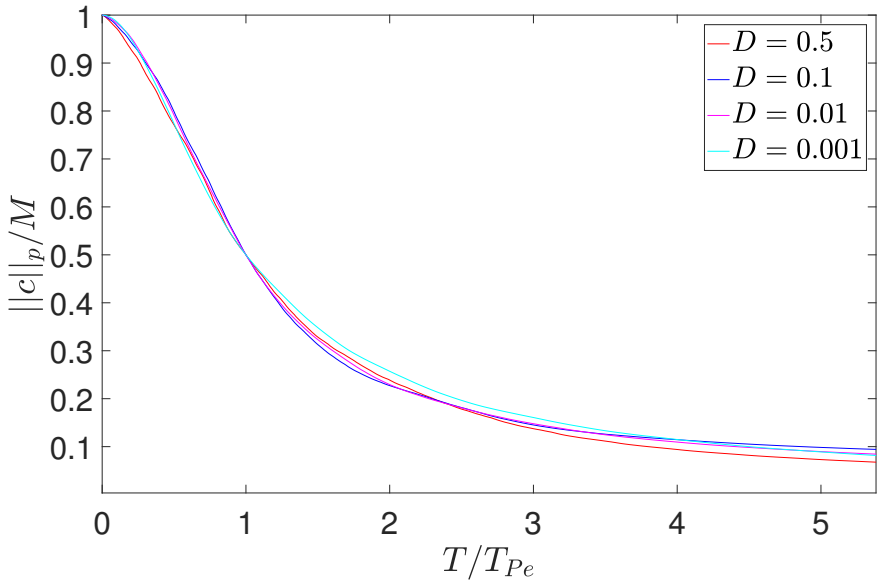

Figure 3.16. Choosing one specific cutting and shuffling dynamical system from Figure 3.13 with parameters $N = 5$, $r = 1.2$, and $\Pi = [52413]$, and computing the decay of the mixing norm for ever smaller diffusivities $D = 0.5, 0.1, 0.01, 0.001$.

Though Figure 3.13 shows the relaxation of the line segment's color to the mean through *many different* mixing protocols, it is clear that (after the appropriate rescaling) all IETs with diffusion behave in a *universal* way. Therefore, we conclude that there is clear numerical evidence of the existence of a "cut-off phenomenon" in the set of dynamical systems that we have constructed. However, to "prove" such a cut-off, we need to observe the transition from unmixed to mixed sharpening as D becomes small as in [33].

To this end, in Figure 3.16, we show some select curves from Figure 3.13 as D becomes very small, zooming near $T/T_{Pe} = 1$. There is some sharpening of the transition but a clear conclusion cannot be drawn from this plot. Thus, we conjecture that a physically based estimate of T_{Pe} is needed, rather than the numerical one from Equation (3.7), to clearly define the cut-off. This physically based estimate is the subject of the next section.

3.5 Predicting the Stopping Time T_{Pe}

Schlick *et al.* [55] proposed a simple one-dimensional analysis of diffusion between two subsegments of unequal color (on a normalized domain with given Pe), using the an analytic solution to the diffusion equation [*i.e.*, Equation (2.9)]. (Muzzio and Ottino [56] previously considered the related case of reaction-diffusion.) In [55], the line segment was taken to have length 2ℓ (*i.e.*, each subsegment was of length ℓ), and the colors were taken to be $c_1 = 0$ and $c_2 = 1$ without loss of generality. A solution was developed using eigenfunctions, from which it was determined that a subsegment length of ℓ^*, where

$$\ell^* = \ell^*(\hat{T}) = \pi\sqrt{\frac{\hat{T}}{2Pe}}, \tag{3.8}$$

will be "washed out" in a characteristic normalized/dimensionless time $\hat{T}$ to be made precise below (given a specific Péclet number Pe) [3]. Thus, based on this analysis from [55], we pose the following question: when will the *average* continuous-color subsegment length, denoted ℓ_m, in our cutting and shuffling process *without* diffusion reach ℓ^*? This question

[3]Since Equation (3.8) introduces a length $\ell^* \propto \sqrt{D}$, it can be considered as a type of *Batchelor scale* [46,57], which describes the smallest length scale of fluctuations that can persist in a fluid flow before they are homogenized by molecular diffusion.

is important because, if $\ell_m \simeq \ell^*$ then $\hat{T}$ iterations of the cutting and shuffling *with* diffusion ($D \neq 0$, for a given Pe) later, the concentration of the striation will be damped out (decrease) by $e^{-2} \approx 13.5\%$ [55, p. 15].

For cutting and shuffling without diffusion ($D = 0$), we first rescale the problem as in Section 2.5, which yields the Péclet number definition (using a velocity scale $L/T_{\max}$):

$$Pe = \frac{L^2}{DT_{\max}}. \tag{3.9}$$

Under this rescaling both $\hat{X} := X/L$ and $\hat{T} := T/T_{\max}$ run from 0 to 1. Then, the average subsegment length (*i.e.*, the average of the lengths of subsegments of continuous color) can be trivially shown to be given exactly by

$$\ell_m(\hat{T}) = \frac{1}{\hat{C}(\hat{T}) + 1}. \tag{3.10}$$

Here, as before, $\hat{C}(\hat{T}) := C(T)$ is the number cutting interfaces as defined after $\hat{T}$ normalized iterations so the number of distinct subsegment of continuous color is clearly $\hat{C}(\hat{T})+1$. Next, we seek to estimate the number of iterations $\hat{T}$ required for diffusion to "wash out" the color gradients.

To this end, in Figure 3.17, we show visually how to determine when $\ell^* \simeq \ell_m$. In the absence of diffusion, the number of iterations required for the latter condition to hold is given by the $\hat{T}$ values at the intersections of the ℓ_m and ℓ^* curves in Figure 3.17. At these $\hat{T}$, we can expect that diffusion dominates the dynamics, leveling the concentration gradients. Thus, we would like to argue that these values of $\hat{T}$ are estimates of the stopping times. Let us introduce the notation $\hat{T} = \tilde{T}_{Pe}/T_{\max}$ (with the tilde introduced to clearly distinguish this value from the one in Section 3.4) for this normalized stopping time, which is now defined based on Eqs. (3.8) and (3.10) as the solution of

$$\pi\sqrt{\frac{\hat{T}}{2Pe}} = \frac{1}{\hat{C}(\hat{T}) + 1}. \tag{3.11}$$

Unfortunately, since the number of cutting interfaces $C(T)$ is a complicated function, for which we do not have a closed form solution, Equation (3.11) must be solve numerically.

After obtaining the value of $\tilde{T}_{Pe}/T_{\max}$ numerically from Equation (3.11), we can verify whether the foregoing argument about the influence of diffusion is valid by calculating the mixing norm decay with the specific Pe given initially, from which we immediately get the corresponding diffusion coefficient to be used in a cutting and shuffling simulation:

$$D = \frac{L^2}{Pe\, T_{\max}}. \tag{3.12}$$

To summarize: supposing a Péclet number (inverse dimensionless diffusivity) is known for a line segment of length L normalized to 1, then ℓ^* is estimated by Equation (3.8) based on [55]. Next, the number of normalized iterations $\tilde{T}_{Pe}/T_{\max}$ of the diffusionless ($D = 0$) cutting and shuffling process until diffusion would "take over" is estimated from Equation (3.11), from which $\tilde{T}_{Pe}$ trivially follows. Next, to verify the latter is an estimate of the stopping time, a cutting and shuffling simulation with diffusion is performed, using the properly matched diffusivity according to Equation (3.12).

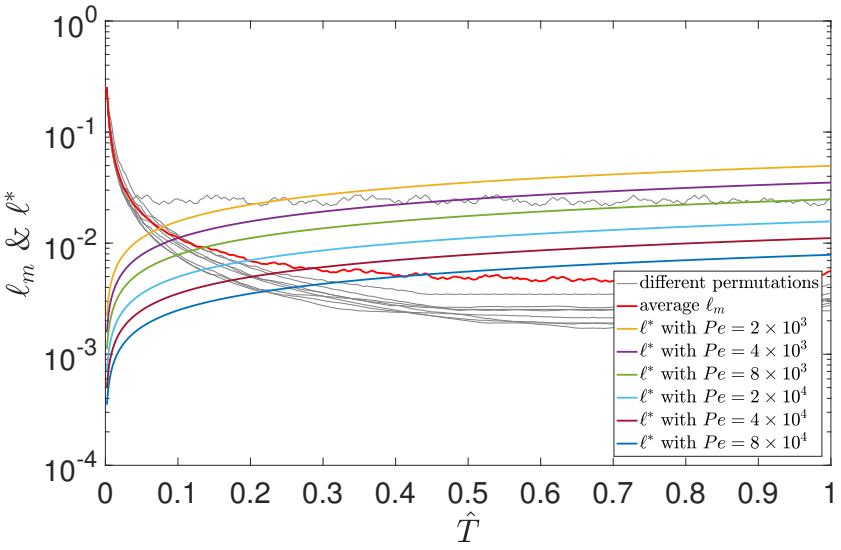

Figure 3.17. Graphical illustration of solving for $\hat{T} = \tilde{T}_{Pe}/T_{\max}$ such that $\ell^*(\hat{T}) = \ell_m(\hat{T})$. The average subsegment length ℓ_m (in the absence of diffusion) is shown as the gray curves for $N = 4$, $r = 1.2$, $T_{\max} = 500$ and $D = 0$ for various Π. The intersections of this averaged curve with the ℓ^* curves (different colors correspond to different Pe values, as in the legend) yield $\tilde{T}_{Pe}/T_{\max} = 0.074, 0.102, 0.136, 0.196, 0.284, 0.408$.

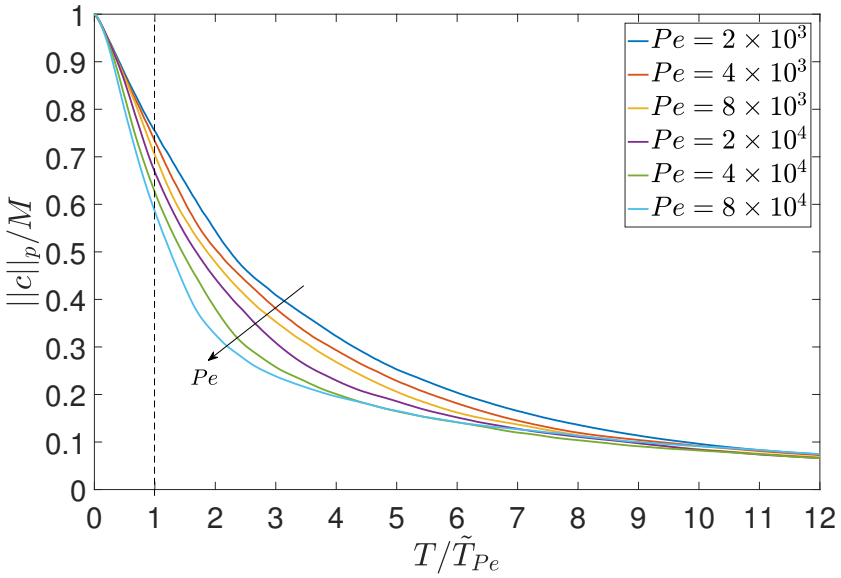

Figure 3.18. Average mixing norm $||c||_p(T)$ with $N = 4$, $r = 1.2$, rescaled using $\tilde{T}_{Pe} = 45.01$, 57.995, 78.995, 124.005, 141.995, 189 for $D = 0.4506$, 0.2253, 0.1126, 0.0563, 0.0375, 0.0282, respectively, as per Figure 3.17.

A result from this numerical approach is illustrated in Figure 3.18 for a select choice of N and r. Clearly, some collapse of the otherwise disparate mixing norm curves is observed against $T/\tilde{T}_{Pe}$ for the estimated values of $\tilde{T}_{Pe}$ obtained from Equation (3.11) and as shown visually in Figure 3.17. More importantly, however, the collapse is "imperfect," specifically showing a "steepening" of the profiles as $Pe \to \infty$. This steepening (as in [33]) is suggestive of a cut-off (sharp transition from a unmixed state to a mixed state), the ideal form of which is represented by the dashed vertical line connecting 1 to 0 at $T/\tilde{T}_{Pe} = 1$ in Figure 3.18.

Figures 3.20 and 3.22 show similar results. In Figure 3.20, we have again $N = 4$ subsegments but with a ratio $r = 1.4$, while in Figure 3.22 we use $N = 5$ and $r = 1.5$. Although less pronounced, the cut-off phenomenon appears to be present in both of these figures, and we have confirmed this is the case for other choices of N and r as well (not shown for brevity). The corresponding estimates, $\tilde{T}_{Pe}$, are obtained in the same way as before and as illustrated in Figures 3.19 and 3.21, respectively. The grouping of the curves is now much tighter, suggesting that the case in Figure 3.18 is, in a sense, "special" in clearly showing

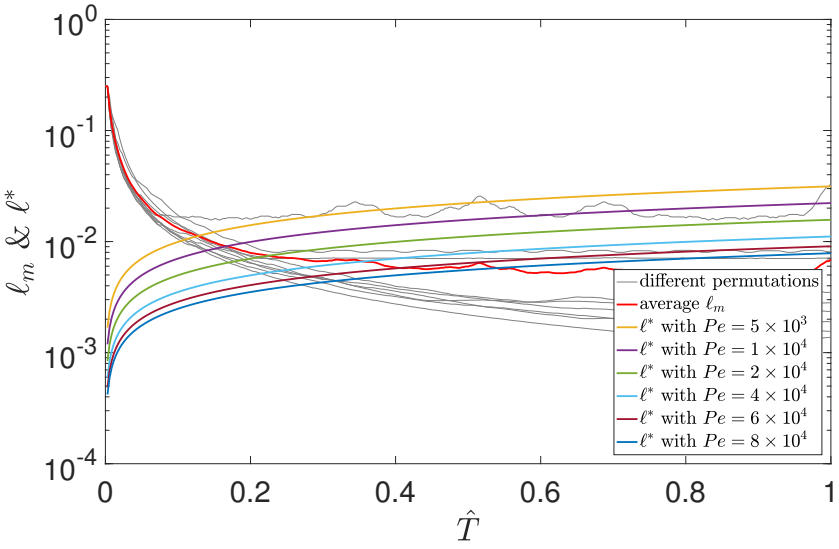

Figure 3.19. Graphical illustration of solving for $\hat{T} = \tilde{T}_{Pe}/T_{\max}$ such that $\ell^*(\hat{T}) = \ell_m(\hat{T})$, as in Figure 3.17, but for $N = 4$, $r = 1.4$, $T_{\max} = 350$ and $D = 0$ for various Π. The intersections of ℓ_m with the ℓ^* curves yield the values of $\tilde{T}_{Pe}/T_{\max} = 0.1286, 0.1657, 0.2257, 0.3543, 0.4057, 0.54$.

the steepening. Nevertheless, a steepening with increasing Pe is observed in Figure 3.20 as well, confirming that the cut-off phenomenon is present for other choices of N and r in our cutting and shuffling process with diffusion.

Finally, having considered the effect of different N and r, we would like to compare the various predictions in the above discussion to understand the relationship between $\tilde{T}_{Pe}$ and Pe. This dependence is shown in Figure 3.23. In general, the estimated stopping time $\tilde{T}_{Pe}$ increases with Pe, which should be expected given the hypothesis of a cut-off phenomenon. However, the specific dependence appears to be sensitive upon the choice of N and r, and no clear pattern emerges. Thus, it remains the subject of future inquiry whether a specific functional form could be determined to specify the relationship between $\tilde{T}_{Pe}$ and Pe *a priori*.

Finally, we consider the relationship between the computed half-mixing time T_{Pe} and the predicted stopping time $\tilde{T}_{Pe}$. Figure 3.24 shows the scatter plot of $\tilde{T}_{Pe}$ values versus T_{Pe} values. In this type of plot of predicted versus expected values, a linear relationship between T_{Pe} and $\tilde{T}_{Pe}$ would signify that the prediction is valid. In Figure 3.24, we observe

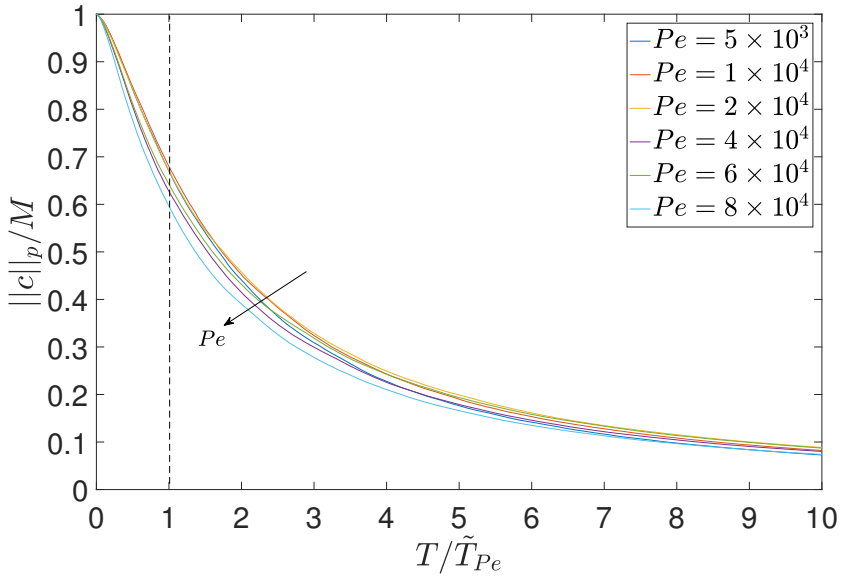

Figure 3.20. Average mixing norm $||c||_p(T)$ with $N = 4$, $r = 1.4$, rescaled using $\tilde{T}_{Pe} = 37, 51, 68, 98, 142, 204$ for $D = 0.45024, 0.22512, 0.11256, 0.045024, 0.022512, 0.011256$, respectively, as per, as per Figure 3.19.

an approximately linear relationship, though the slope is not one. Nevertheless, we can conclude that we can use $\tilde{T}_{Pe}$ to predict the half-mixing time of the system.

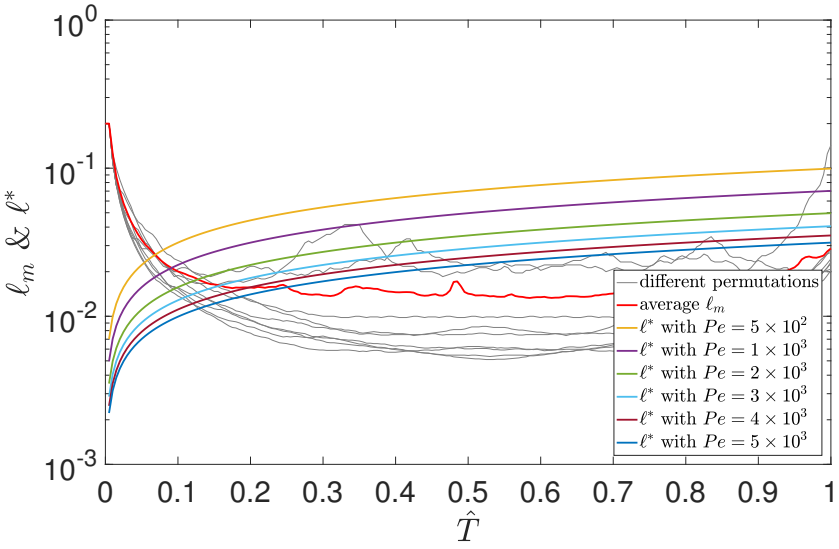

Figure 3.21. Graphical illustration of solving for $\hat{T} = \tilde{T}_{Pe}/T_{\max}$ such that $\ell^*(\hat{T}) = \ell_m(\hat{T})$, as in Figure 3.17, but for $N = 5$, $r = 1.5$, $T_{\max} = 200$ and $D = 0$ for various Π. The intersections of ℓ_m with the ℓ^* curves yield the values of $\tilde{T}_{Pe}/T_{\max} = 0.07, 0.09, 0.13, 0.16, 0.2, 0.25$.

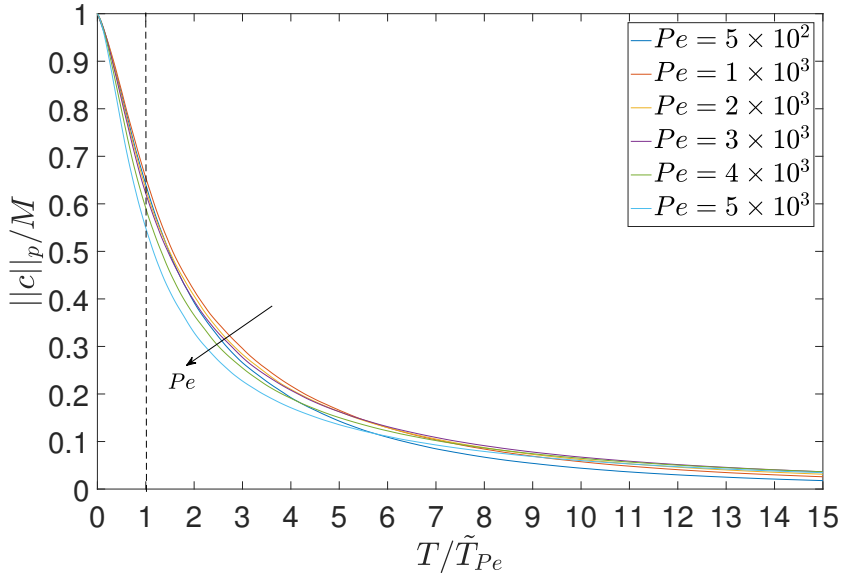

Figure 3.22. Average mixing norm $||c||_p(T)$ with $N = 5$, $r = 1.5$, rescaled using $\tilde{T}_{Pe} = 14, 18, 26, 32, 40, 50$ for $D = 0.4452, 0.2226, 0.1113, 0.0742, 0.0557, 0.0445$, respectively, as per, as per Figure 3.21.

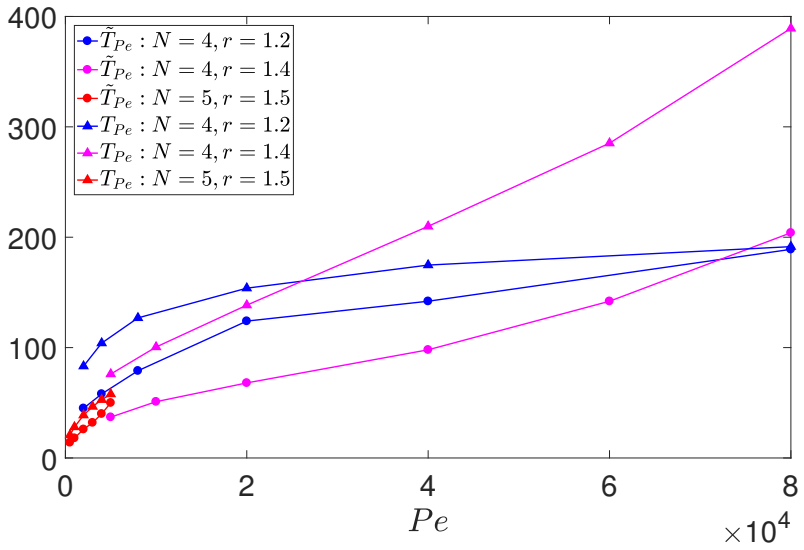

Figure 3.23. The curves with circle symbols show the dependence of the stopping time $\tilde{T}_{Pe}$, as calculated through Equation (3.11), as a function of Pe for three pairs of N and r values. The curves with triangle symbols show the dependence of the stopping time T_{Pe}, as calculated through Equation (3.7), as a function of Pe for same three pairs of N and r values. Lines connecting individual data points are a guide-to-eye.

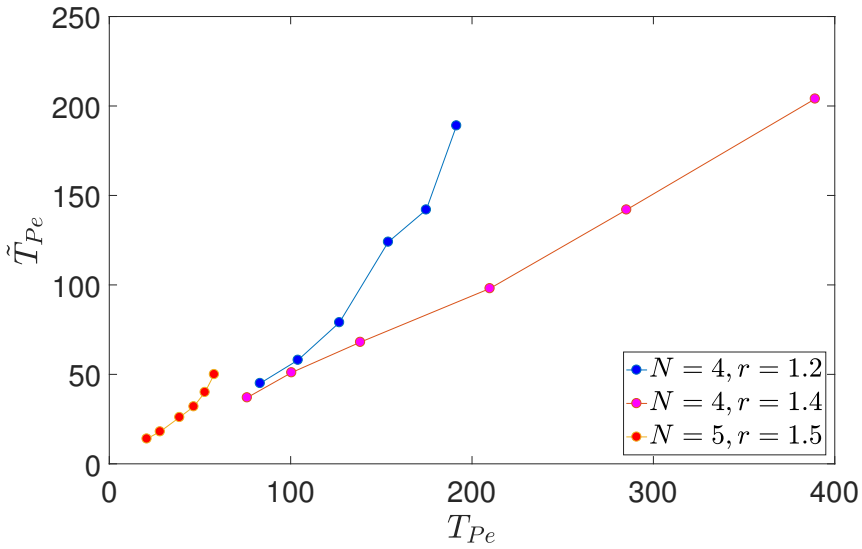

Figure 3.24. Scatter plot for predicted $\tilde{T}_{Pe}$ values, via Equation (3.11), and calculated T_{Pe}, via Equation (3.7), showing an approximately linear scaling of predicted with calculated.

4. CONCLUSIONS

In the present work, we discussed the effects of incorporating diffusion into one-dimensional cutting and shuffling maps represented by interval exchange transformations. The most obvious conclusion is that diffusion leads to significantly enhanced mixing compared to cutting and shuffling alone. However, in the presence of diffusion, we must additionally be careful how we quantify mixing. Specifically, a "mixing norm" is a more effective way to quantify the degree of mixing compared to the number of cutting interfaces, a quantity of interested in the dynamical systems theory of interval exchange transformations.

Next, we proposed a parametrization of the possible mixing behaviors. Indeed, the class of cutting and shuffling protocols considered has a large parameter space: the number of initial subsegments N, the adjacent subsegment length ratio r, the shuffling permutation Π, and the diffusivity D can all be varied independently. Our parametrization consists of fitting the decay of the mixing norm with the number of iterations to two parameters: a time constant τ and a skewness parameter α, which were both found to depend on the ratio r and on the diffusion coefficient D, for fixed N. Through this approach, we showed that, even though a large number of dynamical behaviors are possible, an appropriate rescaling of the mixing norm decay curves leads to a *universal* mixing curve, describing (within some error margin) all cutting and shuffling protocols. This universality rests upon the fact that a number of iteration for the mixing norm to decay by 50%, denoted T_{Pe}, can be defined (and found numerically) for each protocol.

Another question we sought to address is whether cut-offs, and the concomitant concept of stopping times, from finite Markov chain theory apply here. To this end, we sought to determine a critical number of iterations $\tilde{T}_{Pe}$ *the stopping time) at which diffusion would "kick in" thus homogenizing the mixture. In doing so, we explored the limit of vanishing diffusivity (*i.e.*, $Pe \to \infty$), confirming (at least numerically) that the transition from an unmixed stated becomes sharper as $Pe \to \infty$. Thus, we have completed the analogy to cut-

offs and stopping times, which so gracefully explains that a deck of fifty-two cards requires about seven (and not any more) shuffles to become randomized. Of course, unlike card shuffling, interval exchange transformations possess significant complexity. Even tough such maps are easy to describe qualitatively, their mathematical theory remains an advanced and difficult topic in dynamical systems. Our results on cut-offs are also distinct from those by Liang and West [33] because they considered *chaotic* maps in several dimensions, while our interval exchanges are at best weakly mixing (though never truly so since we work on finite grids and with integer arithmetic).

A possible avenue of future work involves extending our cutting and shuffling approach with diffusion to consider chemical reactions occurring between the subsegments of different color. Such an extension could connect to the classical work on evolution and coarsening of lamellar structures in chaotic mixing [20, 44, 56, 58]. (Lamellar models of mixing remain an active topic of research today [59].) The interplay between the lamellar width distribution, coupled to chemical reactions and diffusion processes, plays a key role in the evolution toward a steady state and, thus, the final yield of a chemical reaction. Clifford *et al.* [44] discussed these issues at length, however, overall they initially considered only "simple" initial arrangement. Specifically, Clifford *et al.* noted that a weakness of their approach was that "lamellae can have only two different widths, while realistic fluid flows generate lamellae with a wide range of widths" [44, p. 305]. Meanwhile, earlier work by Sokolov and Bluman concluded that "the course of reaction is governed mainly by mixing and not by diffusion or kinetics." [58, pp. 3698–3699]. Thus, cutting and shuffling a line segment with reaction and diffusion presents a natural model in which to capture such complexity.

As we have shown in the present work, when permutations leading to poor mixing and pathological cases are excluded, the behavior of the remaining protocols of cutting and shuffling with diffusion is, in a sense, universal although the "stopping time" T_{Pe} is highly sensitive to the details of the protocol. Conceivably, such universality persist in the presence of reactions with the stopping time becoming the quantity one may wish to optimize. Indeed, the lamellar distributions under pure reaction and diffusion have been shown to evolve in

a *self-similar* manner [20, 56], suggesting some level of universality already exists in the process. Nevertheless, these remain questions that must be addressed in future work.

Some additional future work can also include examining the sensitivity of the dynamical system to all the parameters. For example, the complexity of adjacent subsegment length ratio r could be varied in a more systematic way than we have here, to determine possible "resonance" or other system behaviors. In combination with the number of subsegments N and diffusivity D, varying r could have nontrivial impact on the mixing behavior of the system. Our work only discussed a small part of the parameter space, focusing on the fundamental effects of incorporating diffusion into cutting and shuffling. Also, since the initial condition is linked to the subsegment ratio r and number of initial pieces/cuts N, another open question is whether there still exists a universal behavior if we start from other/arbitrary initial condition.

REFERENCES

REFERENCES

[1] A. Goetz. Dynamics of piecewise isometries. *Illinois J. Math.*, 44:465–478, 2000.

[2] A. Goetz. Piecewise isometries — an emerging area of dynamical systems. In P. Grabner and W. Woess, editors, *Fractals in Graz 2001*, pages 135–144. Birkhäuser, Basel, 2002.

[3] J. H. B. Deane. Piecewise isometries: Applications in engineering. *Meccanica*, 41:241–252, 2006.

[4] J. M. Ottino. *The Kinematics of Mixing: Stretching, Chaos, and Transport*. Cambridge University Press, Cambridge, 1989.

[5] R. Sturman, J. M. Ottino, and S. Wiggins. *The Mathematical Foundations of Mixing*, volume 22 of *Cambridge Monographs on Applied and Computational Mathematics*. Cambridge University Press, Cambridge, 2006.

[6] S. Wiggins and J. M. Ottino. Foundations of chaotic mixing. *Phil. Trans. R. Soc. Lond. A*, 362:937–970, 2004.

[7] G. Juarez, R. M. Lueptow, J. M. Ottino, R. Sturman, and S. Wiggins. Mixing by cutting and shuffling. *EPL*, 91:20003, 2010.

[8] I. C. Christov, J. M. Ottino, and R. M. Lueptow. Streamline jumping: A mixing mechanism. *Phys. Rev. E*, 81:046307, 2010.

[9] I. C. Christov, J. M. Ottino, and R. M. Lueptow. From streamline jumping to strange eigenmodes: Bridging the Lagrangian and Eulerian pictures of the kinematics of mixing in granular flows. *Phys. Fluids*, 23:103302, 2011.

[10] G. Juarez, I. C. Christov, J. M. Ottino, and R. M. Lueptow. Mixing by cutting and shuffling 3D granular flow in spherical tumblers. *Chem. Eng. Sci.*, 73:195–207, 2012.

[11] I. C. Christov, R. M. Lueptow, and J. M. Ottino. Stretching and folding versus cutting and shuffling: An illustrated perspective on mixing and deformations of continua. *Am. J. Phys.*, 74:359–367, 2011.

[12] P. P. Park, P. B. Umbanhowar, J. M. Ottino, and R. M. Lueptow. Mixing with piecewise isometries on a hemispherical shell featured. *Chaos*, 26:073115, 2016.

[13] L. D. Smith, P. P. Park, P. B. Umbanhowar, J. M. Ottino, and R. M. Lueptow. Predicting mixing via resonances: Application to spherical piecewise isometries. *Phys. Rev. E.*, 95:062210, 2017.

[14] D. H. Kelley and N. T. Ouellette. Separating stretching from folding in fluid mixing. *Nat. Phys.*, 7:477–480, 2011.

[15] L. D. Smith, M. Rudman, D. R. Lester, and G. Metcalfe. Mixing of discontinuously deforming media. *Chaos*, 26:023113, 2016.

[16] L. D. Smith, M. Rudman, D. R. Lester, and G. Metcalfe. Impact of discontinuous deformation upon the rate of chaotic mixing. *Phys. Rev. E.*, 95:022213, 2017.

[17] L. D. Smith, P. B. Umbanhowar, J. M. Ottino, and R. M. Lueptow. Mixing and transport from combined stretching-and-folding and cutting-and-shuffling. *Phys. Rev. E.*, 96:042213, 2017.

[18] R. Sturman, S. W. Meier, J. M. Ottino, and S. Wiggins. Linked twist map formalism in two and three dimensions applied to mixing in tumbled granular flows. *J. Fluid Mech.*, 602:129–174, 2008.

[19] M. K. Krotter, I. C. Christov, J. M. Ottino, and R. M. Lueptow. Cutting and shuffling a line segment: Mixing by interval exchange transformations. *Int. J. Bifurcation Chaos*, 22:1230041, 2012.

[20] F. J. Muzzio and J. M. Ottino. Evolution of a lamellar system with diffusion and reaction: A scaling approach. *Phys. Rev. Lett.*, 63:47–50, 1989.

[21] A. Katok and B. Hasselblatt. *Introduction to the Modern Theory of Dynamical Systems*, volume 54 of *Encyclopedia of Mathematics and Its Applications*. Cambridge University Press, Cambridge, 1995.

[22] M. Yu, P. B. Umbanhowar, J. M. Ottino, and R. M. Lueptow. Cutting and shuffling of a line segment: Effect of variation in cut location. *Int. J. Bifurcation Chaos*, 26:1630038, 2016.

[23] L. D. Smith, P. B. Umbanhowar, J. M. Ottino, and R. M. Lueptow. Optimized mixing by cutting-and-shuffling. 2018. preprint arXiv:1803.08102, http://arXiv.org/abs1803.08102.

[24] Ya. G. Sinai and C. Ulcigrai. Weak mixing in interval exchange transformations of periodic type. *Lett. Math. Phys.*, 74:111–133, 2005.

[25] A. Avila and G. Forni. Weak mixing for interval exchange transformations and translation flows. *Ann. Math.*, 165:637–664, 2007.

[26] W. de Melo, B. Poonen, J. Quastel, and A. Zorich. The work of the 2014 Fields medalists. *Not. AMS*, 62:1334–1349, 2015.

[27] L. N. Trefethen and L. M. Trefethen. How many shuffles to randomize a deck of cards? *Proc. R. Soc. Lond. A*, 456:2561–2568, 2000.

[28] D. Aldous and P. Diaconis. Shuffling cards and stopping times. *Am. Math. Monthly*, 93:333–348, 1986.

[29] P. Diaconis. The cutoff phenomenon in finite markov chains. *Proc. Natl. Acad. Sci.*, 93:1659–1664, 1995.

[30] P. Diaconis and L. Saloff-Coste. Separation cut-offs for birth and death chains. *Ann. Appl. Probab.*, 16:2098–2122, 2006.

[31] G. Kolata. In shuffling cards, 7 is winning number. *New York Times*, January 9, 1990.

[32] J. B. Keller. How many shuffles to mix a deck? *SIAM Rev.*, 37:88–89, 1995.

[33] T.-C. Liang and M. West. Numerical evidence for cutoffs in chaotic microfluidic mixing. In *Proc. ASME 2008 Dynamic Systems and Control Conf.*, pages 1405–1412, New York, NY, 2008. ASME.

[34] A. D. Stroock, S. K. W. Dertinger, A. Ajdari, I. Mezić, H. A. Stone, and F. M. Whitesides. Chaotic mixer for microchannels. *Science*, 295:647–651, 2002.

[35] P. L. Krapivsky, S. Redner, and E. Ben-Naim. *A Kinetic View of Statistical Physics*. Cambridge University Press, Cambridge, UK, 2010.

[36] P. W. Miller and N. T. Ouellette. Impact fragmentation of model flocks. *Phys. Rev. E*, 89:042806, 2014.

[37] P. Ashwin, M. Nicol, and N. Kirkby. Acceleration of one-dimensional mixing by discontinuous mappings. *Physica A*, 310:347–363, 2002.

[38] R. Sturman. The role of discontinuities in mixing. *Adv. Appl. Mech.*, 45:51–90, 2012.

[39] G. Froyland, C. González-Tokman, and T. M. Watson. Optimal mixing enhancement by local perturbation. *SIAM Rev.*, 58:494–513, 2016.

[40] H. Kreczak, R. Sturman, and M. C. T. Wilson. Deceleration of one-dimensional mixing by discontinuous mappings. *Phys. Rev. E.*, 96:053112, 2017.

[41] B. Xu, Y. Li, X. Xu, and X. Xu. Quantitative evaluation of passive scalar flow mixing a review of recent developments. *ChemBioEng Reviews*, 4:120–140, 2017.

[42] J.-L. Thiffeault. Using multiscale norms to quantify mixing and transport. *Nonlinearity*, 25:R1–R44, 2012.

[43] M. Keane. Interval exchange transformations. *Math. Z.*, 141:25–31, 1975.

[44] M. J. Clifford, S. M. Cox, and E. P. L. Roberts. Reaction and diffusion in a lamellar structure: the effect of the lamellar arrangement upon yield. *Physica A*, 262:294–306, 1999.

[45] C. F. Novak. Discontinuity-growth of interval-exchange maps. *J. Mod. Dynam.*, 3:379–405, 2009.

[46] J.-L. Thiffeault. Scalar decay in chaotic mixing. *Lect. Notes Phys.*, 744:3–35, 2008.

[47] P. V. Danckwerts. The definition and measurement of some characteristics of mixtures. *Appl. Sci. Res. A*, 3:279–296, 1952.

[48] J. M. Ottino. The mixing of fluids. *Sci. Am.*, 260:56–67, 1989.

[49] S. Wiggins. Stirred but not mixed. *Nature*, 333:395–396, 1988.

[50] R. T. Pierrehumbert. Tracer microstructure in the large-eddy dominated regime. *Chaos Solitons Fractals*, 4:1091–1110, 1994.

[51] J. Strikwerda. *Finite Difference Schemes and Partial Differential Equations*. Society for Industrial and Applied Mathematics, 2nd edition, 2004.

[52] Y. Fan, P. B. Umbanhowar, J. M. Ottino, and R. M. Lueptow. Shear-rate-independent diffusion in granular flows. *Phys. Rev. Lett.*, 115:088001, 2015.

[53] K. L. McIlhany and S. Wiggins. Optimizing mixing in channel flows: kinematic aspects associated with secondary flows in the cross-section. *Microfluid Nanofluid*, 10:249–262, 2010.

[54] J. C. Phillips. Stretched exponential relaxation in molecular and electronic glasses. *Rep. Prog. Phys.*, 59:1133–1207, 1996.

[55] C. P. Schlick, I. C. Christov, P. B. Umbanhowar, J. M. Ottino, and R. M. Lueptow. A mapping method for distributive mixing with diffusion: Interplay between chaos and diffusion in time-periodic sine flow. *Phys. Fluids*, 25:052102, 2013.

[56] F. J. Muzzio and J. M. Ottino. Dynamics of a lamellar system with diffusion and reaction: Scaling analysis and global kinetics. *Phys. Rev. A*, 40:7182–7192, 1989.

[57] G. K. Batchelor. Small-scale variation of convected quantities like temperature in turbulent fluid Part 1. General discussion and the case of small conductivity. *J. Fluid Mech.*, 5:113–133, 1959.

[58] I. M. Sokolov and A. Blumen. Reactions in systems with mixing. *J. Phys. A: Math. Gen.*, 24:3687–3700, 1991.

[59] M. Souzy, I. Zaier, H. Lhuissier, T. Le Borgne, and B. Metzger. Mixing lamellae in a shear flow. *J. Fluid Mech.*, 838:R3, 2018.